Title

Increased post-mitotic senescence in aged human neurons is a pathological feature of Alzheimers disease.

Journal

Cell Stem Cell, 29(12)

Authors

Herdy, Joseph
Traxler, Larissa
Agarwal, Ravi
et al.

Publication Date

2022-12-01

DOI

10.1016/j.stem.2022.11.010

Peer reviewed

HHS Public Access

Author manuscript

Cell Stem Cell. Author manuscript; available in PMC 2023 April 12.

Published in final edited form as:

Cell Stem Cell. 2022 December 01; 29(12): 1637–1652.e6. doi:10.1016/j.stem.2022.11.010.

Increased post-mitotic senescence in aged human neurons is a pathological feature of Alzheimer's disease

Joseph R. Herdy[1,2,3,*], **Larissa Traxler**[3], **Ravi K. Agarwal**[2], **Lukas Karbacher**[2], **Johannes C.M. Schlachetzki**[4], **Lena Boehnke**[3], **Dina Zangwill**[2,5], **Doug Galasko**[1], **Christopher K. Glass**[4], **Jerome Mertens**[2,3,*], **Fred H. Gage**[2,6,*]

[1]Department of Neurosciences, University of California, San Diego, La Jolla, CA, USA

[2]Laboratory of Genetics, The Salk Institute for Biological Studies, La Jolla, CA, USA

[3]Neural Aging Laboratory, Institute of Molecular Biology, CMBI, Leopold-Franzens-University Innsbruck, Tyrol, Austria

[4]Department of Cellular and Molecular Medicine, University of California, San Diego, La Jolla, CA, USA

[5]Division of Biological Sciences, University of California, San Diego, La Jolla, CA, USA

[6]Lead contact

SUMMARY

The concept of senescence as a phenomenon limited to proliferating cells has been challenged by growing evidence of senescence-like features in terminally differentiated cells, including neurons. The persistence of senescent cells late in life is associated with tissue dysfunction and increased risk of age-related disease. We found that Alzheimer's disease (AD) brains have significantly higher proportions of neurons that express senescence markers, and their distribution indicates bystander effects. AD patient-derived directly induced neurons (iNs) exhibit strong transcriptomic, epigenetic, and molecular biomarker signatures, indicating a specific human neuronal senescence-like state. AD iN single-cell transcriptomics revealed that senescent-like neurons face oncogenic challenges and metabolic dysfunction as well as display a pro-inflammatory signature. Integrative profiling of the inflammatory secretome of AD iNs and patient cerebral spinal fluid revealed a neuronal senescence-associated secretory phenotype that could trigger astrogliosis in human astrocytes. Finally, we show that targeting senescence-like neurons with senotherapeutics could be a strategy for preventing or treating AD.

[*]Correspondence: jherdy@salk.edu (J.R.H.), jerome.mertens@uibk.ac.at (J.M.), gage@salk.edu (F.H.G.).

AUTHOR CONTRIBUTIONS

Conceptualization: J.R.H., J.M., and F.H.G.; methodology: J.R.H., J.M., R.K.A., L.K., D.Z., L.T., L.B., J.C.M.S.; software: J.R.H., J.M.; formal analysis: J.R.H., J.M., L.T., R.K.A., J.C.M.S., L.B., L.K.; investigation: J.R.H., J.M., L.T., R.K.A., D.Z., J.C.M.S., L.B.; resources: J.M., F.H.G., C.K.G., J.C.M.S., D.G.; data curation: J.R.H., J.M., L.K.; writing – original draft: J.R.H., J.M., F.H.G.; writing – review and editing: J.R.H., J.M., F.H.G.

SUPPLEMENTAL INFORMATION

Supplemental information can be found online at https://doi.org/10.1016/j.stem.2022.11.010.

DECLARATION OF INTERESTS

F.H.G. is an advisory board member of *Cell Stem Cell*.

INCLUSION AND DIVERSITY

We support inclusive, diverse, and equitable conduct of research.

Graphical Abstract

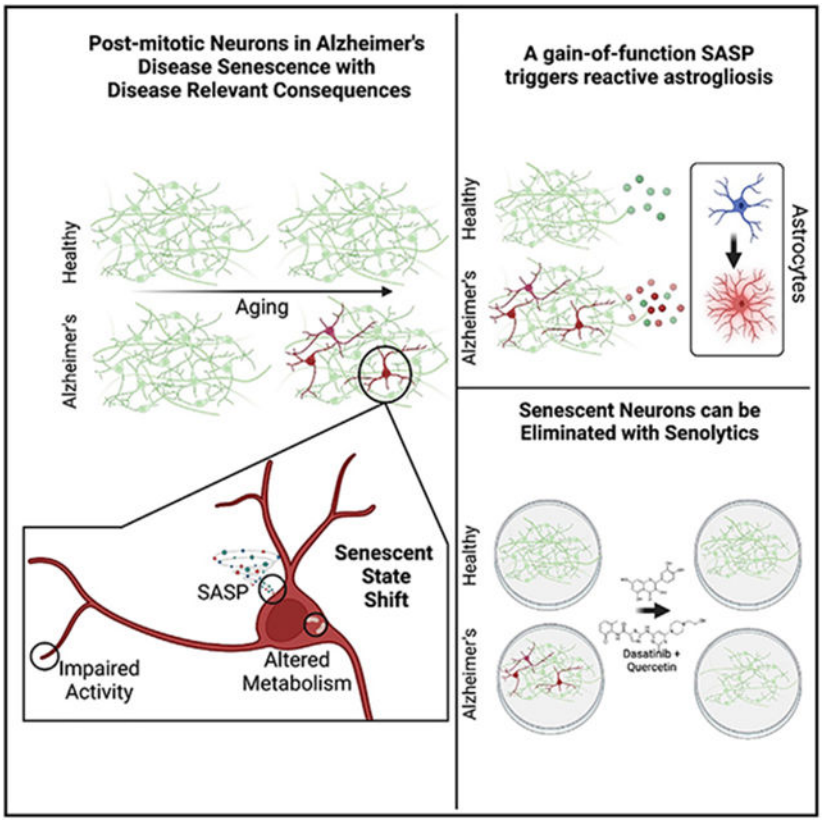

In brief

Herdy et al. identify an enriched population of senescent neurons in the Alzheimer's brain, which can be modeled *in vitro* using induced neurons (iNs) and eliminated with senotherapeutics. Alzheimer's iNs present molecular and genetic markers of senescence and an inflammatory secretome that can trigger reactive astrogliosis.

INTRODUCTION

The integration of mature, terminally differentiated neurons into elaborated networks is thought be one of the fundamental principles of neuronally encoded information in the brain. Across a human lifetime, neurons face immense evolutionary pressure to retain this post-mitotic, differentiated state indefinitely to preserve information. Lifelong terminal differentiation is not without cost, however, and the inability to rejuvenate cellular components combined with the longevity of humans leads to the accumulation of numerous defects late in life, including DNA damage, mitochondrial dysfunction, epigenetic changes, and transcriptional drift.[1,2] When confronted with these late-life cellular stressors, cells may undergo a process known as cellular senescence. Senescent cells increase in abundance during aging, where they contribute to tissue dysfunction and numerous age-related disorders.[3] Recent studies have changed the perception of cellular senescence, expanding it from a response to serial passage to a central role in responding to stress, molecular

damage, and oncogene activation. Importantly, post-mitotic neurons experience many of the same age-related stressors that trigger senescence in proliferating cells. Indeed, there are a growing number of recent reports of senescence-like signatures in non-dividing cells, including osteoclasts,[4] mature adipocytes,[5] neurons,[6] and others.[7] Like proliferating cells, senescence in neurons is linked to aging and cellular stress, yet there is an important gap in knowledge regarding the definition and understanding of the senescence-like state of aged human neurons.

Despite decades of research, Alzheimer's disease (AD) remains a debilitating, progressive, and ultimately fatal dementia with no disease-modifying treatment options. The vast majority of cases (>95%) are sporadic, with no known cause aside from advanced age.[8] As the population over age 65 grows, the burden of AD is destined to grow in lockstep. As early as the 1990s, several observations were made that suggested neuronal senescence might be a feature of AD, but the prevailing view that senescence was restricted to proliferating cells limited the impact of this work.[9,10] However, the growing reports of a senescence-like phenotype in neurons in a variety of aging or injury contexts led to the hypothesis that aged human neurons can enter a senescence-like state and contribute to AD pathology.

RESULTS

The human pre-frontal cortex of AD patients harbors an increased proportion of senescent neurons

The CDKN2A gene, which encodes the senescence-activating proteins p16INK4a and p14ARF, is consistently upregulated in senescent cells and is considered to be one of the most specific genetic markers of senescence.[11] Therefore, we examined CDKN2A expression in post-mortem brains from 30 AD patients and 99 sex- and age-matched cognitively normal (NC) controls from the Allen Aging, Dementia, and Traumatic Brain Injury (TBI) study. We found that CDKN2A mRNA abundance was significantly increased in the neuron-rich pre-frontal cortex (PCx) of AD patients (Figure 1A)[12]; by contrast, no CDKN2A expression changes were detected in the frontal white matter (FWM), which contains mostly axons and glia (Figures 1A and S1A). CDKN2A expression also trended higher in other neuron-rich areas of AD patients, and CDKN2A increased in expression during aging in the human brain (Figures S1B-C). Given the field's evolving understanding of cellular senescence as a phenomenon whose features can materialize in non-dividing cells late in life[7] and the reports of neuronal senescence in rodents and humans,[9,13] we asked whether neurons contribute to increased CDKN2A expression in the PCx. We obtained PCx brain tissue from a clinically characterized cohort of mid-stage AD patients (Braak III–IV, n = 10) and age-/sex-matched NC controls (n = 10) and performed fluorescence immunohistochemistry for p16INK4a (p16) and the mature neuron marker NeuN (Figure 1B and Table S1). Remarkably, we observed a distinct subpopulation of NeuN/p16 double-positive neurons in all aged brains, and these cells were significantly (about 3-fold) more abundant in AD brains (Figures 1B and 1C). NeuN/p16 double-positive cells represented a minority of NeuN-positive cells, and the majority of p16-positive cells in the brain were NeuN negative (Figure 1C). The sparse number of p16-positive cells is consistent with the general view that senescent cells represent a minority within their resident tissue and

supports the notion that senescent neurons are less abundant than senescent glia.[14] Further, these rates are consistent with a recent eigen-gene approach to estimate the abundance of senescent neurons in the cortex of AD patients.[15] Due to bystander effects, senescent cells tend to cluster in their resident niche,[16] so we examined p16 clustering by calculating adjacency scores of p16 in reference to NeuN or DAPI loci.[17] As expected, p16 localization showed a clear clustering pattern, with p16 foci significantly closer to their nearest neighbor than a randomized subsampling of tissue loci (Figures 1D and 1E). Notably, p16-positive cells were significantly more likely to cluster around NeuN-positive cells, indicating that senescent-like neurons represent a potential source for secreted bystander factors and might act as a starting point for senescent cell clusters in the aged human brain. This effect appeared to be neuron specific, as we detected significantly weaker clustering of p16 near DAPI foci than NeuN loci (Figure 1D). Further, clustering tended to be elevated in AD (Figure S1D). These data suggest that neurons expressing p16INK4a are more common in the brains of AD patients and that senescent-like cells, including neurons, tend to cluster together in a pattern consistent with bystander senescence initiation.

Senescent transcriptomic and epigenomic patterns in age-equivalent AD iNs

Given the increased abundance of p16-expressing neurons in AD patient brains, we next sought to examine the extent to which aged induced neurons (iNs) from AD patients display senescence-related features. To functionally assess the molecular features of senescence in human neurons in AD, we generated iNs from a cohort of AD patients and non-demented controls. Briefly, we obtained punch biopsies from AD 16 (13 sporadic, 3 familial) patients and 19 non-demented controls (CTL)for iNs. It has been shown that donor-specific iNs capture age- and disease-specific molecular pathologies, including transcriptomic, mitochondrial, and epigenetic aging signatures in aging iNs,[18,19,20] cell fate instability in AD iNs,[21] and other phenotypes.[22,23,24] Our cohort includes patients aged 57–88 (Figure 2A and Table S5), and control donors were further matched according to age, sex, and ApoE genotypes to mitigate genetic bias. Following direct Ngn2-/Ascl1-mediated iN conversion for 21 days and polysialic acid-neural cell adhesion molecule (PSA-NCAM) fluorescence-activated cell sorting (FACS)-based purification, we obtained mature cortical iNs as previously reported[19,20,21,25,26] (Figure S2A), with equivalent efficiency in AD and CTL lines (Figures S2B-C). To explore AD-associated changes in senescence gene expression in AD iNs, we collected whole-transcriptome RNA-sequencing (RNA-seq) data from the iNs (n = 35). To identify changes specific to aged neurons, we also prepared RNA-seq from three control groups: (1) isogenic induced pluripotent stem cell (iPSC)-derived neurons (iPSC-iNs) that appear transcriptionally fetal relative to a human brain development atlas (n = 20); (2) the corresponding unconverted fibroblasts (n = 35); and (3) unconverted iPSC lines from the same cohort (n = 20) (Figure 2A).[27,28] Differential expression analyses of AD vs. CTL for all four cell types (iNs, iPSC-iNs, fibroblasts, and iPSCs) were ranked separately according to significance then log2FC for gene set enrichment analysis (GSEA) of a list of canonical senescence genes (reactome R-HSA-2559583). Interestingly, we observed a strong and significant enrichment of senescence genes exclusively in AD iNs but no significant enrichment in rejuvenated AD iPSC-iNs, fibroblasts, or iPSCs (Figures 2B and 2C). Importantly, senescence genes are predominantly upregulated in AD iNs and include 33 significantly upregulated genes such as the classic senescence and inflammation

markers CDKN2A, MMP3, CXCL8, CXCL5, CDKN1C, and interleukin-6 (IL-6). Only three were significantly downregulated.[29] Notably, two of these three downregulated senescence genes also have neuron-specific functions (NMDA receptor-associated RAB5B gene and the neuronal morphogenesis IGSF3 gene), which might explain why they are not upregulated (Figure 2C).[21,30,31] Senescence genes were also significantly upregulated in iNs relative to iPSC-iNs for all patients, highlighting the adult-specific and age-dependent nature of this activation (Figure S2D). To validate and better characterize the relative contribution of senescence genes in human neurons, we integrated our iN transcriptome data with RNA-seq data of human embryonic stem cell-derived neurons where senescence was induced by KO of SATB1.[32] In addition to a significant loss of SATB1 expression in AD iNs, rank rank hypergeometric order (RRHO) analysis confirmed the hypothesis that AD iNs are transcriptionally closer to senescent SATB1-knockout (KO) neurons than to wild-type (WT) neurons (Figure S2E). Next, we examined the overlap in genes that were significantly differentially expressed between both AD and CTL iNs and SATB1 KO and WT neurons, which revealed 59 co-upregulated and 44 co-downregulated genes (padj < 0.05). Gene ontology (GO) analysis of upregulated genes identified a significant enrichment of genes related to extracellular matrix (ECM) reorganization, including metallopeptidases (ADAMTS5), collagenases (COL11A1), and glypicans (GPC4). Thus, endogenous transcriptional activation of a neuronal senescence gene expression profile is specific to aged human neurons and enriched in neurons from AD patients. The neuronal senescence profile is characterized by functional genetic markers of senescence, including increased CDKN family expression, ECM modification, and inflammatory gene expression.

In response to aging-related stress, state transition toward senescence is known to be deeply anchored in epigenomic landscape changes that establish senescence-associated gene expression. To assess whether the increased expression of senescence genes in AD neurons is founded in their epigenomes, we examined chromatin accessibility using assay for transposase-accessible chromatin sequencing (ATAC-seq) of PSA-NCAM purified iNs (n = AD 10; 11 CTL) and CpG DNA methylation (DNAm) status using the Illumina MethylEPIC chip (n = AD 8; 8 CTL). ATAC-seq revealed that senescence genes were markedly more accessible in AD iNs, consistent with their higher gene expression, with an average of 31% more peaks per gene (Figure 2D). Similarly, average promoter DNAm in CTL iNs inversely correlated with expression on a gene-by-gene basis and showed the expected overall negative relationship between promoter methylation and expression of senescence genes (Figure 2E). Interestingly, increased methylation of senescence gene promoters in AD iNs appeared to be insufficient to dampen their expression, and AD samples counterintuitively displayed an overall positive correlation of promoter methylation to gene expression (Figure 2E). At the same time, overall senescence gene promoter methylation was largely similar in both groups (Figure S2F). Thus, as high promoter methylation is typically associated with decreased expression,[33] these findings indicate a disruption of gene regulation by promoter methylation in senescence genes of AD iNs. Next, to specifically assess neuron-specific functions that are rooted in epigenetic and transcriptomic changes, we filtered for all the genes that showed increased promoter ATAC-seq accessibility, lower promoter methylation, and increased RNA-seq expression exclusively in the AD iNs, but not in fibroblasts from the same patients (n = 1,225 genes). We then performed GSEA, which revealed that five of the

top 20 enriched pathways were senescence-related terms, including oxidative stress-induced senescence, DNA damage-induced senescence, and the senescence-associated secretory phenotype (Figure 2F). Consistently, many gene sets were shared with ATAC-seq data from SATB1-KO neurons, further indicating a compromised neuronal chromatin landscape (Figure S2G).[32] This notion is supported by analysis of the replication-independent histone variant H2AFJ, which is preferentially upregulated in senescent cells.[34] H2AFJ transcripts, as well as its associated gene targets, were significantly upregulated in AD iNs (Figure S2H), and immunocytochemistry of H2AFJ revealed significantly brighter H2AFJ staining in AD iNs (Figure 2G). We next probed for potential key upstream effectors in our ATAC-seq data that had the potential to override DNAm marks and drive senescent gene expression in AD iNs. We found that regions containing the binding motif for the transcription factor ETS1 were significantly more open in AD iNs (Figure 2H), and ETS1 is known to drive expression of p16INK4a and bind both hypo- and hyper-methylated promoters in replicative senescence.[35,36] Thus, ETS1 is a tangible example of a factor that can drive senescence gene expression despite increased promoter methylation in human neurons (Figure 2H).

Although we did not observe substantial senescence gene activation in fibroblasts and used passage-equivalent lines in our experiments, telomere attrition during fibroblast passaging might contribute to a compromised neuronal chromatin landscape. Therefore, we sought to determine whether iN senescence was independent of telomere attrition by measuring telomere content by qPCR in PSA-NCAM-purified AD and CTL iNs (n = AD 9; 9 CTL) across 22 population doublings (passages 10–32). No significant difference in the rate of telomere attrition between AD and CTL was detected in the fibroblasts (Figure 2I). Likewise, the average absolute telomere content per genome was unchanged (234 kb in AD and 228 kb in control iNs).[37,38] Another independent estimation of population doublings by CpG methylation indicated no significant difference in doublings of iN or parent fibroblast lines (Figure S2I).[39] Telomere shortening may occur in replication-independent scenarios upon downregulation of the telomere factor *POT1* and shelterin subunit *TERF2*; however, we observed no difference in the expression of these two genes in AD and CTL iNs (Figure S2J).[40]

Taken together, these data indicate that a compromised epigenetic landscape in AD iNs, including relaxation of chromatin at senescence genes, upregulation of a senescence-related histone, dysregulation of methylation at senescence promoters, and ETS1 transcription factor binding, contributes to the increased expression of senescence genes in AD neurons, and this expression is independent of telomere attrition and not a “carryover” of proliferative senescence in parent fibroblasts.

AD iNs mirror post-mortem neuronal senescence of patient brains and present *bona fide in vitro* markers of cellular senescence

Because an increased fraction of NeuN-positive cells in the AD patient brains expressed p16 and CDKN2A mRNAs were upregulated in AD iNs, we next sought to examine the p16 protein in our iN model (Figure S3A). Consistently, a capillary western blot analysis of protein extracted from PSA-NCAM-purified iNs confirmed increased p16 protein levels in AD iNs (Figure 3A). Immunocytochemical analysis showed that AD iNs had significantly

more p16-positive cells and a higher fluorescence intensity of p16 staining within the positive fraction (Figure 3B). Notably, the 3-fold increase in the number of p16-positive neurons in AD iNs over controls was remarkably similar to what we observed in post-mortem tissue, though the overall abundance of senescent neurons was larger *in vitro* than *in vivo* by 4-fold. These results suggest that iNs faithfully recapitulate the senescence activation observed in NeuN-expressing cells in the AD brain and that iNs can be used to model spontaneous neuronal senescence *in vitro*.

We next explored whether AD iNs present classic biomarkers of senescence. First, we tested for the common senescence marker senescence-associated beta galactosidase (BGal).[13,41] Consistently, AD iNs were significantly more likely to be BGal positive than control iNs (Figure 3C), and no increased BGal abundance was observed in parallel fibroblast cultures (Figure S3B). Importantly, neuronal senescence appeared to be largely independent of the number of BGal-positive cells in the fibroblast culture or the donor ages at biopsy, as neither rate correlated with the fraction of BGal-positive iN cultures (Figure S3C). We also observed no significant differences in senescence marker abundance when comparing sex as a biological variable in our cohort (Figures S3D-E). As a secondary measure of BGal activity, we used a C_{12}FDG strategy that offers a fluorogenic readout of BGal activity that can be measured via FACS. We observed clear population separation between C_{12}^{+} and C_{12}^{-} in PSA-NCAM^{+} cells, and AD iNs had a significantly larger C_{12} population than CTL lines measured in a subset of our cohort (n = 8) (Figure 3D). Because other characteristic features of senescent cells are increased cytoplasmic and nuclear volumes,[3] we extracted cellular volumes from forward scatter area (FSC-A) data and measured the nuclear area of purified iNs by DAPI staining. Indeed, FSC-A values were substantially higher (Figure S3F), and region of interest (ROI)-based nuclear areas were significantly larger in AD iNs compared with controls (Figure 3E), and AD nuclei tended to be larger in post-mortem tissue, though not significantly (Figure S1E). Two common changes accompanied by alterations in nuclear size in senescent cells are the loss of lamin B1 in the nuclear envelope and the formation of senescence-associated heterochromatin foci (SAHF). We examined AD and CTL iN lines for these two markers but did not detect any differences in lamin B1 (Figure S3G) or the formation of SAHF (data not shown); these markers may be more common features of senescence in replicative cells.

We next sought to test whether senescence markers were specific to aged neurons or whether they also appeared in young neurons from the same patients. Matched PSA-NCAM-purified iPSC-iNs from three AD patients from our cohort lacked BGal signal and p16 immunoreactivity (Figures 3F and 3G). Consistently, p16 mRNA was not detected in iPSC-iNs by RNA-seq (Figure 3H). These data, together with the low level of senescent gene expression observed in iPSC-iNs (Figure S2D), suggest that senescence activation is more likely to occur in aged neurons and that rejuvenated fetal-like iPSC-iNs have lower rates of spontaneous senescence under baseline culture conditions (Figure 3I).

Single-cell transcriptomics reveal a neuronal senescence trajectory that culminates in oncogenic challenges and metabolic dysfunction in senescent-like neurons

Similar to the aged brain, iN cultures from AD and CTL donors show a high degree of heterogeneity with regard to various senescence markers. Thus, some genetic features specific to the minority of senescent neurons might be masked in our initial bulk transcriptome data from AD 16 patients and 19 CTLs. To capture mosaic transcriptional features that describe the path from normal to a senescent-like neuron and to extract the key features of fully senescent neurons, we performed single-cell transcriptome analysis of non-FACS-purified AD and CTL iN cultures (Figure 4A). In this one case, we opted to perform single-cell RNA sequencing (scRNA-seq) on unsorted cultures that contain a mixture of iNs and unconverted fibroblasts, in contrast with all other previous experiments on PSA-NCAM-purified neurons, to minimize the viability loss caused by flow sorting. We retrieved reliable libraries from 29,515 cells (n = AD 4, 3 CTL, Table S2), and we employed a partition-based graph abstraction strategy to resolve transcriptional topology using Monocle3.[42] Uniform manifold approximation and projection (UMAP) dimensionality reduction identified five transcriptionally distinct clusters in our dataset after filtering for low-quality cells (Figures 4B and S4A). As anticipated, we observed undifferentiated and only partially converted fibroblasts that separated from successfully converted iNs based on UMAP clustering. These were characterized by low expression of neuronal fate genes and high expression of fibroblast fate genes (Figure S4B). Further, RNA trajectory analysis indicated a clear differentiation continuum from fibroblast to neuron identity (Figure S4C), with one cluster capturing fully converted iNs. Pseudo-bulk differential expression analysis between the fibroblast cluster and iN cluster significantly correlated with the transcriptome profiles of bulk fibroblasts vs. iNs (Figure S4E), and the fraction of cells allocated to the iN cluster was also consistent with the percentage of stringent PSA-NCAM-positive neurons typically observed during FACS purification (Figure S5D). AD and CTL iNs differentiated at equal efficiencies, and there was no significant difference in the correlation of AD or CTL iNs to fibroblast gene expression. Finally, we assessed the transcriptional neuronal subtype identity within the iN cluster, and consistent with bulk data, we found that most iNs expressed glutamatergic or GABAergic markers but virtually no dopaminergic, cholinergic, or serotonergic cells (Figure S4F).

Next, we sought to isolate senescent from non-senescent cells within the iN cluster by assigning cells a senescent module score. On the pseudo-bulk level, AD iNs had a higher overall senescence module score than CTLs, but no significant difference was detected in fibroblasts (Figures 4C and S5A). We separated the top and bottom 15% of module-scored iNs to obtain sen-high and sen-low bins and performed differential expression analysis (Figure 4D). Sen-low and sen-high iNs significantly differed in their expression of CDKN2A, indicating that our scoring approach was successful (Figure S5B). Unbiased differential expression analysis of the sen-low and sen-high populations revealed 865 genes that were significantly differentially expressed (q value < 0.05) as well as 644 upregulated genes and 221 downregulated in sen-high iNs (Figures 4D and S5C). GSEA of these genes revealed that senescence in neurons is accompanied by decreased expression of synaptic and neuronal functionality genes, indicating that in human neurons the senescent state underlies compromised cellular functionality (Figure 4E). Further, we detected changes

in gene sets for major metabolism pathways in senescent iNs, with a significant loss of oxidative phosphorylation and citric acid cycle (TCA) electron transport (Figure 4E). Notably, senescent-like iNs showed a significant gain in the expression of several functional gene sets, including genes related to ECM organization, DNA damage repair pathways, and pro-inflammatory senescence-associated secretory phenotype (SASP).[43] Although these are all classic features of cellular senescence in other cell types, the marked increase in SASP-related mRNA abundance in iNs was surprising. Importantly, this SASP signature was absent from fibroblasts and occurred specifically in iNs from AD patients (Figure S5F). We hypothesize that neurons themselves might secrete SASP factors, which could explain the bystander effects observed in post-mortem AD brain tissues, and that senescent neurons might trigger pro-inflammatory cascades in AD.

To evaluate molecular features specific to senescence in AD neurons, we contrasted AD from control iNs that binned into sen-low and sen-high groups (Figure S5D). Interestingly, differential expression analysis detected more transcriptional differences between AD and control iNs in the sen-high group (n = 227 genes) than in the sen-low group (n = 62 genes), and 36 genes were shared between the groups (Figure S5D). Next, we examined putative functional protein-protein interaction networks of genes upregulated in AD iN in sen-high and sen-low groups separately. Two distinct networks were upregulated in sen-low: (1) neuron development (including terms related to morphogenesis, nephron development, and nervous system development) and (2) metabolic changes (including nucleoside metabolism, ATP synthesis, and electron transport chain). In contrast, sen-high AD iNs gained a pro-inflammatory transcriptional network with a trio of cytokine- and interleukin-related terms, as well as a significantly expanded network of metabolic changes (Figure 4F). This finding indicates that, in non-senescent neurons, AD iNs experience initial metabolic changes and neuron development challenges that proceed to an expanded metabolic reprogramming and inflammatory activation after senescence induction. To further examine the senescence trajectory in aged human neurons, we employed reverse graph embedding to order single cells along a pseudotime corresponding to increased CDKN2A expression, allowing us to examine genes that changed across this trajectory and the relative abundance of patient populations (Figure 4G). Consistent with their increased senescence score, AD iNs were overrepresented at late, high CDKN2A pseudotimes (Figure 4H). In addition to CDKN2A, CDKN1D and CDKN1C followed this trajectory of increased expression across pseudotime. Notably, CDKN1A was the exception, as its expression fell at late pseudotimes. Interestingly, CDKN1A is known to be active early in senescence and to decrease during late senescence when other genes such as CDKN2A become active, suggesting that this pattern is maintained in senescence in neurons.[44] Other genes that increased across senescence pseudotime include potent inflammatory genes, including CXCL5/8, CST5, and IL7 (Figures 4H and S5E).

Finally, we sought to validate these results in an independently generated post-mortem AD scRNA-seq dataset (Figure S5G).[45] We extracted 6,369 excitatory neurons from this dataset (4,725 AD, n = 11 and 1,644 healthy, n = 7), as excitatory neurons are reported to be the most prone to senescence-related changes in AD. Cells were then arranged in pseudotime corresponding to increased CDKN2A expression, where we again observed an overrepresentation of AD neurons at late, high-senescence pseudotimes.

Likewise, inflammatory gene expression, matrixmodifying genes, and co-expression of CDKN family members followed a similar trajectory in post-mortem neurons as iNs. Differential expression analysis across senescence pseudotime captured gene networks related to neurodegeneration and loss of functional synaptic genes, as well as metabolic dysfunction with the loss of cyclic adenosine monophosphate (cAMP) signaling (Figure S5H). The prominent loss of synapse-related genes further suggests that senescent neurons have impaired function both *in vitro* and *in vivo*. Thus, both a scoring and reverse graph-embedding approach identified increased senescence gene expression in AD iNs, suggesting that early vs. late senescence in neurons can be distinguished by initial metabolic and oncogenic challenges that culminate in a pro-inflammatory response and metabolic reprogramming in deep senescence.

AD iN SASP-conditioned media triggers astrogliosis

A minority of senescent cells can have an outsized impact on tissue homeostasis through paracrine pro-inflammatory SASP molecules,[29] and reactive astrogliosis is now widely considered to be one of the defining pathological features of AD.[46] Our scRNA-seq data indicate that deep neuronal senescence is characterized by a pro-inflammatory SASP-related gene expression signature specifically in AD iNs, and we wondered whether AD iNs were capable of releasing SASP factors into the media, which could trigger astrogliosis. We obtained cerebrospinal fluid (CSF) from a cohort of 184 patients (n = AD 102, 82 NC) and separately prepared conditioned media (CM) from six AD and six CTL PSA-NCAM-purified iN cultures. We measured inflammation traces using a proximity extension assay based on oligonucleotide-linked antibodies (Figure 5A). Remarkably, 21 of the 40 overlapping probes showed the same direction of change between AD and CTL patient samples from both CSF and iN CM samples, indicating that these signaling factors were indeed released by neurons in an AD-specific manner (Figure 5B and Table S3). Notably, AD patients' CSF had increased levels of known SASP proteins, including CXCL5/6/9, CCL23/11, IL7, and MMP10.[47] CST5, an inflammatory factor recently described to be active at the earliest stages following TBI, was also upregulated in both CSF and iN samples.[48] Furthermore, three of the identified upregulated proteins in AD CSF and AD iNs (MMP10, STAMBP, and EIF4EBP1) were previously discovered as AD biomarkers.[49] To directly assess whether AD iN-derived SASP factors were a sufficient source to trigger astrocyte reactivity, we exposed healthy ApoE3 homozygous primary human cortical astrocytes, which expressed the appropriate receptors for our identified inflammatory targets, to CM from AD and control iN cultures (Figures 5A,S6A-B, and S6E-F). Interestingly, both AD and control iN CM triggered an increase in $GFAP^+$ area, indicating that the secretome of aged human iNs was sufficient to activate human astrocytes. Importantly, we observed that the AD iNs, but not fibroblast or iPSC-iNs, CM-initiated a hyperreactive state in the astrocytes, which was evident from higher $GFAP^+$ area and significantly brighter GFAP signals (Figures S6B-D). Although higher GFAP is associated with astrocyte reactivity, it is also expressed in non-reactive astrocytes. To validate and further assess astrocyte reactivity in response to AD iN-derived SASP factors, we assessed the transcriptomes of human astrocyte cultures by RNA-seq exposed to either control or AD iN CM. Differential expression analysis identified 1,071 genes upregulated and 981 genes downregulated in astrocytes in response to AD iN CM (padj < 0.05, abs[log2FC] > 1) (Figure 5C). Genes

known to characterize reactive astrogliosis were widely upregulated following exposure to AD CM, including genes related to the cytoskeleton (nestin, vimentin), metabolism (ALDOC, FABP7), chaperones (CRYAB), secreted proteins (C3, Serpina3n, IL6), signaling receptors (NTRK2, IL17R), and downregulation of glutamate transporters (EAAT1/2) (Figure 5D).[50] Interestingly, the most significantly downregulated gene was TIMP3, a matrix metalloprotease inhibitor whose targets include MMP10, one of the factors we identified as significantly increased in AD CSF and secreted by AD iNs.[51] Next, we mapped our data to scRNA-seq data from post-mortem tissue astrocytes extracted from patients with or without AD pathology.[52] We found that 177 of the 537 geneures that were differentially expressed (padj < 0 .05, log2FC > 1) in AD astrocytes *in vivo* were also significantly differentially expressed after exposure to AD CM, including loss of glutamate transporters and synapse-related genes (Figure S6G and Table S4). Consistently, RRHO of the log2FC-ranked differentially expressed genes between AD and CTL iN CM-treated astrocytes compared with post-mortem astrocytes with or without AD pathology found a 1.662-fold increase in control and a 1.625-fold increase in AD gene enrichment in response to AD CM (Figure 5F).

Because SASP factors can not only trigger inflammatory cascades but also elicit bystander senescence in neighboring cells, we were curious whether AD iN CM-treated astrocytes would themselves enter a senescent state. To test this, we compared astrocyte transcriptome profiles with non-senescent vs. irradiation-induced senescent astrocytes.[53] Interestingly, we found that 83% of the genes whose expression significantly changed after exposure to AD CM were also significantly differentially expressed in senescent astrocytes. Likewise, RRHO indicated that AD CM-treated astrocytes appeared transcriptionally closer to senescent astrocytes than non-senescent controls (1.21- and 1.2-fold enrichment, respectively) (Figure S6H). Together, these results suggest that senescent human neurons can trigger neighboring neurons as well as astrocytes to enter senescence in response to pro-inflammatory SASP factors that are specifically secreted by AD iNs. Further, neuronal paracrine effects trigger a disease-related reactive pro-inflammatory transcriptomic response and senescent astrocytic state that closely mirror those of reactive astrocytes in the diseased human brain, including cytokine release, loss of synaptic maintenance, changes in metabolism, and morphological changes (Figure 5E).

Senescence in neurons can be triggered by oncogenes and eliminated with senotherapeutics

A wide variety of cellular stressors can trigger senescence, but whether these are sufficient to induce senescence in neurons is largely unexplored. Our previous study found that AD iNs experience an oncogenic challenge and de-differentiation stress, and oncogenic stress is one of the most robust methods for senescence induction.[21,54] Therefore, we tested whether overexpression of an oncogene could trigger oncogene-induced senescence (OIS) in iNs. Following differentiation, iNs were transduced with a lentivirus for the overexpression of KRasG12V:GFP, an oncogenic form of the Ras gene used widely to trigger senescence, or a GFP control virus (Figure 6A).[55] After a week of transgene overexpression, cells were fixed and stained for p16 and NeuN to assess activation of senescence in neurons. Similar to reports in proliferating cells, Ras-induced iNs had significantly higher amounts

of p16-positive cells compared with GFP controls (Figure 6B). Importantly, this senescence activation was not accompanied by a loss of neuronal fate, and proportions of NeuN-positive cells did not differ between Ras- or GFP-treated groups (Figure S7A). Further, we did not observe the formation of SAHF in Ras-induced cells that are characteristic of OIS in proliferating cells, indicating that a full DNA damage response (DDR) and consequent establishment of heterochromatin lie downstream of p16 activation, as has been reported.[56] However, it remains possible that longer Ras treatments could culminate in DDR and SAHF formation in neurons. These results confirm that oncogenic Ras is sufficient to produce a senescence response in neurons and that OIS is a robust activator of senescence in both proliferating and non-proliferating cells.

Clearance of senescent cells in the brain has beneficial effects in mouse models of AD,[57-59] and genetic elimination of senescent cells alleviates age-related brain inflammation and cognitive impairment in mice.[60] Pharmacological elimination using the senescent targeting drug combination dasatinib and quercetin (D + Q) has provided similar results.[59] Therefore, we tested whether PSA-NCAM-sorted AD iNs cultures were more sensitive to D + Q treatment than healthy iN cultures. Indeed, iN cultures treated with the D + Q cocktail (0.5–1.5 μM) for 48 h showed significantly higher levels of TUNEL-positive neurons than CTL iNs exposed to the same treatment (Figures 6C and 6D). Although TUNEL-positive cells increased slightly in CTL cultures after D + Q, the change was much less pronounced than in AD patient lines, and doses of D + Q above 1 μM could produce significant differences in apoptosis between AD and CTL lines. We observed that an average of 6.2% of cells were removed at the highest tested concentration of D + Q, lower than the average $p16^{+}$ cells in AD cultures, suggesting that full removal was incomplete and higher doses of D + Q could be necessary to completely eliminate senescent iNs. However, 1.5 μM of D + Q was able to lower p16 abundance in AD cultures to levels comparable to CTL cultures (Figure 6E). Taken together, these results suggest that senolytic drugs can specifically remove senescent neurons and restore senescent neuron abundance in AD neurons to that of healthy controls (Figure 6F).

Neuronal senescence manifests in impaired electrical activity

Electrical activity and the transmission of information are the principal functions of neurons. Entry into senescence typically results in impaired or altered cellular functionality, and our scRNA-seq dataset indicated that senescent neurons lost expression of functional neuron genes. Therefore, we sought to test whether senescent iN cultures had impaired electrical activity by examining spontaneous neuronal spiking by multi-electrode array (MEA). Senescence was induced in aged iN cultures by p16INK4a overexpression, a strategy used to induce senescence both *in vitro* and *in vivo*, and we confirmed senescence activation in iNs by measuring BGal rates in p16-overexpressing cells relative to a GFP control (Figure S8A).[61,62] PSA-NCAM-sorted iN cultures from an aged healthy individual were treated with p16 or GFP control virus and synapsin:dsRed to monitor cultures, and then cells were replated onto polyornithine laminin-coated MEA plates with a feeder layer of support astrocytes (Figure 7A). Field potentials from iNs were recorded in media optimized to replicate physiological conditions in the human brain (Figure S8B). Following a recovery period of two weeks while iNs re-elaborated their dendritic network, GFP:iNs showed a

robust increase in spontaneous activity as assessed by mean firing rate, which could be specifically ablated by treatment with tetrodotoxin (TTX) (Figures 7B and 7D). However, p16:iNs did not recover electrical activity and had significantly lower levels of spontaneous firing than controls by four weeks of recording (Figures 7B and 7C). Notably, there were no significant differences between spiking of GFP:iNs and p16:iNs when triggered to fire by electrical stimulation (Figure 7E), suggesting that the capacity to fire is preserved in senescent neurons, but their spontaneous activity is decreased relative to controls under baseline unstimulated conditions. Taken together, these results confirm that a consequence of senescence in neurons is impaired spontaneous firing, which could manifest as disruption in information processing in the brain.

DISCUSSION

The concept of cellular senescence has evolved substantially since its original formulation as a proliferative arrest of human skin cells *in vitro*. The evidence of senescent cells across tissues of aged animals highlights senescence as a conventional strategy for responding to age-related stress in many cell types. Conversely, senescent cells have been observed early in development before extensive age-related changes have occurred, and recent studies have uncovered functional roles of senescent cells in regeneration and in response to wound healing.[63,64] These observations suggest a coordinated and programmed cellular state induced by senescence that is dynamic but tightly regulated. Indeed, current knowledge favors a model where transient and controlled induction of senescent cells is adaptive, but accumulation or chronic persistence of these cells results in dysfunction. The explicit cause for the increased prevalence of senescent cells late in life is still a subject of investigation, but it is likely due to a variety of other molecular changes associated with aging, including epigenetic changes, oxidative stress, DNA damage, and proteotoxic stress, all molecular hallmarks that are also shared with neurodegenerative diseases like AD. Here, we report that there is an increased burden of senescent neurons in the brains of AD patients, that we can model these cells *in vitro* using an aged human neuron culture system, and that senescent neurons constitute a neurogenic source of late-life brain inflammation in AD. The consequences of the presence of even a small population of senescent neurons in advanced ages could be quite profound for brain function. A single neuron can make many thousands of connections to its neighbors through extensive synaptic networks, providing ample opportunity for SASP-mediated dysfunction to spread.[65]

Our observations of senescent neurons in the AD brain led us to examine senescent features in aged AD neurons *in vitro* using iNs. Our characterization is consistent with a multi-marker strategy recommended to identify senescent cells with more accuracy.[66] As in other cell types, senescence in neurons results in cellular dysfunction, including reduced spontaneous activity. Reports of senescence in non-dividing cells have occasionally come into conflict with the original conception of senescence as a state limited to proliferating cells, yet cells exhibiting features of senescence have been reported in many non-dividing cell types. Post-mitotic neurons are perhaps the most extensively reported non-dividing cell type to exhibit senescence phenotypes, and they are largely associated with aging or disease-related stress.[14,32,41,58,67] We have shown that aged AD neuron cultures gain an inflammatory SASP that is capable of triggering reactive astrogliosis and that the

transcriptional changes observed in these astrocytes resemble previously reported changes in post-mortem AD astrocytes. Much of the literature surrounding senescence in the brain has identified astrocytes as the cell type that most frequently presents features of senescence.[68,69] The SASP is known to induce senescence in a paracrine manner in neighboring cells, and it is tempting to speculate that the increased prevalence of senescent astrocytes in AD is due at least in part to a senescence-triggering SASP released by nearby senescent neurons. Indeed, our AD CM-treated astrocytes exhibit many of the transcriptional changes seen in irradiation-induced senescence in human astrocytes from a previous study.[53] Thus, a neurogenic, irreconcilable inflammatory response driven by a minority of SASP-releasing neurons could be a potent source of AD-related neuroinflammation seen even at the earliest stages of AD progression.

Ultimately, we show that p16-expressing iNs can be eliminated with a senolytic cocktail of D + Q, reducing the number of p16-expressing cells in AD cultures to a level comparable with CTL cultures. The removal of chronic or overabundant senescent cells from the tissues of aged animals is generally associated with improvements in function and tissue homeostasis, and genetic elimination of senescent cells improved cognitive function of mice late in life, suggesting that targeting senescent cells in the AD brain for elimination could be a novel approach for slowing neuroinflammation and subsequent neurodegeneration in AD. However, given the reports of senescent cells involved in wound healing and regeneration, we stress that more experiments will be necessary to understand the contributions that senescent neurons make to AD pathogenesis or what the ultimate consequences of removing these neurons would have on overall brain function.

There are many known triggers for senescence induction. Previously, we reported that induced neurons from our AD cohort had a loss of neuronal identity and appeared hypomature, expressed many genes associated with cancer, and had metabolic changes resembling a neoplastic Warburg shift.[21,70] These changes are especially pronounced in the cells undergoing senescence in our system. Among other potential causes for a senescence response preferentially in AD neurons, our data support the notion that de-differentiation stress is sufficient to trigger enough of a cell cycle response in a subset of neurons that they commit to the senescent phenotype, and cell cycle re-entry has been proposed as a molecular feature of AD.[71-73] Indeed, challenging healthy neurons with oncogenic Ras produced a senescence response, implicating a common strategy of senescence activation in both proliferating and non-proliferating cells to cancerous transformation. Early in life, during wound healing and regeneration, transient senescence is beneficial, and recent studies suggest that senescence activation late in life could be an attempt to re-activate the wound-healing process.[74] For reasons that are not fully understood, during aging this process goes awry and senescent cells persist and ultimately contribute to tissue dysfunction. Therefore, there is also a possibility that neurons attempting to repair AD-related damage senesce, but in the context of the aged brain, they are incapable of repairing the damage and eventually contribute to an inflammatory feedback loop. Given the complexity of both the activation of senescence and the senescent phenotype itself, more studies will be necessary to fully evaluate senescence in neurons and AD.

LIMITATIONS OF THE STUDY

Fibroblasts to induced neuron conversions are heterogeneous and produce mixed populations of successfully converted neurons and a subset of undifferentiated cells. Here, we used a FACS strategy to isolate neurons from unconverted fibroblasts, and we stress that pure populations be used for evaluation of senescence in these cells as fibroblasts, which readily senescence, have the potential to mask signal originating from neurons. Further, our p16 overexpression strategy produced a large proportion of senescent neurons, which is likely larger than proportions present physiologically in the brain. Finally, despite the relatively large size of our clinically characterized cohort, there is the potential that our sample size might not fully represent the entirety of AD patient diversity.

STAR★METHODS

RESOURCE AVAILABILITY

Lead contact—Further information and requests for resources and reagents should be directed to and will be fulfilled by the lead contact, Fred H. Gage (gage@salk.edu).

Materials availability—All unique and stable reagents generated in this study of which sufficient quantities exists are available from the Lead Contact with a complete Materials Transfer Agreement. Direct conversion lentiviral plasmids have been deposited to Addgene #127288 (pLVX-UbC-rtTA-Ngn2:2A:Ascl1) and #127289 (pLVX-UbC-rtTA-Ngn2:2A:EGFP).

Data and code availability—The accession number for the bulk fibroblast, iPSC, iPSC-iN, and iN RNA-Seq and ATAC-Seq raw data generated in this paper is ArrayExpress: E-MTAB-10352. The accession number for the DNAm EPIC array raw data generated in this paper is ArrayExpress: E-MTAB-10344. The accession number for bulk RNA-Seq from conditioned media treated astrocytes generated in this paper is Sequence Read Archive: PRJNA898624. The accession number for the single cell RNA-Seq generated in this paper is Sequence Read Archive: PRJNA898624. This paper does not report original code. Any additional information required to reanalyze the data reported in this paper is available from the lead contact upon request.

EXPERIMENTAL MODEL AND SUBJECT DETAILS

Subjects—Subjects were participants at the Shiley-Marcos Alzheimer's Disease Research Center (ADRC) at UCSD and provided written informed consent; all procedures were approved by local human subjects committees. Both AD and control subjects underwent rigorous clinical assessment as part of the ADRC study, including detailed neuropsychological testing and brain imaging (MRI), and the subjects selected for biopsies were stratified to show either a clear non-demented clinical picture or clear phenotype of AD (classified as probable AD until pathological confirmation). They were followed for at least 2 years after biopsy with no evidence of cognitive decline (controls) and with evidence of progressive impairment (AD). Punch skin biopsies were obtained at the Altman Clinical & Translational Research Institute (ACTRI) at UCSD, and fibroblast derivation

was performed by standard procedures in serum-containing media. Additional familial AD fibroblast lines were described previously,[80] and 4 old control and 3 young control fibroblast lines were obtained from Coriell (Baltimore longitudinal study of aging) and also described previously.[20,77] Table S1 contains post mortem PFC slice information, and Table S5 indicates which subjects were used for each experiment.

Astrocytes—Human cortical, cerebellar, and hippocampal astrocytes were acquired from a commercial vendor and cultured in astrocyte medium according to the manufacturer's specifications (ScienCell 1800, 1801). For CM experiments, 48-h iN conditioned supernatant was pooled from six AD and six CTL iN lines and spiked in at a 1:3 ratio with untreated astrocyte medium for 48 h. Protein input between pooled samples was normalized to total protein as measured by qubit (ThermoFisher). Cells were then fixed for ICC or harvested with Trizol for RNA extraction.

Fibroblasts and iNs—Primary human dermal fibroblasts from donors between 0 and 88 years of age were obtained from the Coriell Institute Cell Repository, the University Hospital in Erlangen and Shiley-Marcos Alzhiemer's Disease Research Center. Protocols were previously approved by the Salk Institute Institutional Review Board and informed consent was obtained from all subjects. Fibroblasts were cultured in DMEM containing 15% tetracycline-free fetal bovine serum and 0.1% NEAA (Thermo Fisher Scientific) transduced with lentiviral particles for EtO and XTP-Ngn2:2A:Ascl1 (E + N2A) or the combined tetOn system cassette consisting of the rtTAAdv [Clonech] driven by the UbC promoter, Ngn2:2A:Ascl1 under control of the TREtight promoter [Clontech], and a puromycin-resistance gene driven by the PGK promoter (UNA, Figure S2A) and expanded in the presence of G418 (200 μg/mL; Thermo Fisher Scientific) and puromycin (1 μg/mL; Sigma Aldrich), or puromycin only, respectively, as 'iN-ready' fibroblast cell lines. Following at least 3 passages after viral transduction, 'iN-ready' fibroblasts were trypsinized and pooled into high densities (30,000–50,000 cells per cm^2; appx. a 2:1–3:1 split from a confluent culture) and, after 24h, the medium was changed to neuron conversion (NC) medium based on DMEM:F12/Neurobasal (1:1) for three weeks. NC contains the following supplements: N2 supplement, B27 supplement (both 1x; Thermo Fisher Scientific), doxycycline (2 μg/mL, Sigma Aldrich), Laminin (1 μg/mL, Thermo Fisher Scientific Scientific), dibutyryl cyclic-AMP (100 μg/mL, Sigma Aldrich), human recombinant Noggin (150 ng/mL; Preprotech), LDN-193189 (500 nM; Fisher Scientific Co) and A83-1 (500 nM; Santa Cruz Biotechnology Inc.), CHIR99021 (3 μM, LC Laboratories), Forskolin (5 μM, LC Laboratories) SB-431542 (10 μM; Cayman Chemicals), pyrintegrin (1 μM; Tocris), ZM336372 (0.175 μM; Cayman), AZ960 (0.1 μM; Cayman), and KC7F2 (7.5 μM; Fischer Scientific). Medium was changed every third day. For further maturation up to six weeks, iNs were switched to BrainPhys (STEMCELL Technologies)-based neural maturation media (NM) containing N2, B27, GDNF, BDNF (both 20 ng/mL, R&D), dibutyryl cyclicAMP (100 μg/mL, Sigma Aldrich), doxycycline (2 μg/mL, Sigma-Aldrich) and laminin (1 μg/mL, Thermo Fisher Scientific). Formaturation on astrocytes for morphological analysis and calcium imaging, iNs were carefully trypsinized during week 4 and replated on a feeder layer of mouse astrocytes and cultured in NM media containing 2% KOSR (Thermo Fisher Scientific).

iPSCs and iPSC-iNs—Human iPSCs were reprogrammed using the four Yamanaka factors transferred using the Cyto-Tune Sendai reprogramming kit (Invitrogen) or standard retroviral vectors as previously described,[21] and cultured as colonies on Geltrex (Thermo Fisher)-coated plates in iPS-Brew (Miltenyi Biotec). For iPSC-iN transgene delivery, iPSCs were transferred to a monolayer PluriPro (Cell Guidance Systems) condition, transduced with lentiviral particles for pLVX-UbC-rtTA-Ngn2:2A:EGFP (UNG), and expanded in the presence of puromycin (0.5 mg/mL; Sigma Aldrich) as 'iPSC-iN-ready' iPSC-UNG lines as previously described.[76] To initiate conversion, confluent iPSC-UNG monolayer cultures were transferred into NC media to achieve neuronal conversion of the cultures within 3 weeks before fixing and staining, or isolation by flow cytometry for RNA purification.

METHOD DETAILS

Flow cytometry—For isolation of iNs and iPSC-iNs from three-week cultures, cells were detached with TrypLE (Thermo Fisher) and stained for PSA-NCAM directly conjugated to APC (Miltenyl Biotec, 1x) for 1 h at 4C in sorting buffer (250 mM myo-inositol and 5 mg/mL polyvinyl alcohol in PBS) containing 1% KOSR (Thermo Fisher). Cells were washed and resuspended in sorting buffer containing EDTA and DNAse and filtered using a 40-um cell strainer. For C_{12}FDG analysis, cells were first treated with 100 nM bafilomycin A1 for 1 h in fresh culture medium at 37C, 5% CO_2. Next, a 2 mM C_{12}FDG solution was added to the cell culture medium for a final concentration of 33 uM and incubated for an additional hour. Cells were then washed twice with PBS and detached with TrypLE and prepared for FACS as described above.

Immunofluorescence—Formalin-fixed, paraffin-embedded slices of human pre-frontal cortex tissue were obtained from the Shiley-Marcos Alzheimer's Disease Research Center. Slides were deparaffinized and heat antigen retrieval was performed in 10 mM Sodium Citrate buffer (pH 6.0). Slides were permeabilized by two 10-min washes in PBS with 0.4% Triton X-100 (PBS-T) and 1% serum, followed by a 1-h block in PBS-T and 5% serum. Primary antibodies (Mouse NeuN MAB377 1:1000, Rabbit p16INK4a EPR1473 1:1000) were diluted with 1% serum in PBS and incubated at room temperature for 1 h, followed by an overnight incubation at 4C in a humidified chamber. Sections were then washed twice in PBS-T for 10 min followed by secondary antibody (Donkey Anti-Mouse IgG Alexa Fluor 488 and Donkey Anti-Rabbit IgG Alexa Fluor 555, both 1:250) incubation for 2 h at room temperature. Sections were then stained for nuclei with DAPI (1:10,000 Sigma-Aldrich) and washed twice for 10 min with PBS-T. After washing, slides were mounted and coverslips sealed with nail polish.

Cells were cultured on tissue culture-treated ibidi μ-slides for imaging. Cells were fixed with 4% PFA for 20 min at room temperature and washed 3 × 15 min with TBS, followed by a 1-h block with TBS containing 10% serum and 0.1% Triton X-100. Primary antibodies (H2AFJ provided by Carl Mann 1:200, p16INK4a Abcam 1:250, TuJ Covance 1:3000, NeuN EMD Millipore 1:250, GFAP EMD Millipore 1:1000) were applied overnight at 4C. Following two 10-min washes with TBS, nuclei were stained with DAPI (1:10,000 Sigma-Aldrich) and secondary antibodies (Donkey Anti-Mouse IgG Alexa Fluor 488/555 and Donkey Anti-Rabbit IgG Alexa Fluor 488/555, and Donkey Anti-Chicken IgG Alexa

Fluor 488/555, all 1:250) were incubated for 2 h at room temperature. After washing, slides were mounted in PVA-DAPCO (Sigma Aldrich). TUNEL staining was performed with the Click-iT Plus TUNEL Assay 594. SA-B-Gal staining was performed with the Biopioneer cellular senescence detection kit (CS-001). Confocal images were taken on standard fluorescence microscopes or Zeiss LSM780 confocal microscopes.

ImageJ software analyze particles was used for regions of interest (ROI) selection and quantification of immunofluorescent signals within ROIs. Proximity analysis was performed with MorphoLibJ. All data for one experiment were acquired from cells cultured or tissue processed in parallel on the same microscope with the exact same setting used.

Whole genome mRNA-seq and analysis—Total bulk RNA was extracted from fibroblasts and iPSCs and from flow cytometry-isolated iNs and iPSC-iNs following three weeks of conversion using Trizol LS reagent (Thermo Fischer), followed by TURBO DNase digestion (Agilent). RNA integrity was assessed before library preparation using the TruSeq Stranded mRNA Sample Prep Kit according to the manufacturer's instructions (Illumina). Libraries were sequenced paired-end 125 bp using the Illumina HiSeq 2500 platform. Read trimming was performed using TrimGalore, read mapping was performed using STAR, raw counts were generated using HOMER, and variance stabilizing transformation normalization (vst) and differential expression analyses were performed in DESeq2. Statistical values were corrected for false discovery rates (FDR) using the Benjamini-Hochberg method implemented in R. Transcripts per million for all samples were generated by RSEM using standard paired-end or single-end settings as appropriate. CDKN2A, NeuN, and GFAP expression in postmortem human brain samples from the Allen Brainspan Atlas (https://www.brainspan.org/static/download.html) and Aging, Dementia, and TBI study (https://aging.brain-map.org/rnaseq/search) was based on FPKM and differential expression analysis of NeuN, GFAP and CDKN2A was performed using DESeq2 with the default test (Wald test). Analysis of CDKN2A expression across aging was performed with a simple regression analysis t-test in R. Donor metadata for the Aging, Dementia and TBI study can be found here: https://aging.brain-map.org/download/index, and metadata for the Allen Brainspan Atlas at http://help.brain-map.org/display/devhumanbrain/Documentation. Rank Rank Hypergeometric Overlap (RRHO) was performed using the UCLA online tool.

For single cell RNAseq, following three weeks of conversion bulk cultures were harvested with TrypLE without sorting and 10,000 cells per patient were loaded in parallel and processed using the 10x Single Cell 3′ v3 protocol (Illumina). Libraries were prepared following the manufacturer's protocol. Briefly, cells were partitioned into Gel Beads in Emulsion in the GemCode/Chromium instrument followed by cell lysis and barcoded reverse transcription of mRNA, followed by amplification, shearing, and 5′ adapter and index attachment. cDNA was amplified for 11 cycles, and the resulting whole transcriptome was measured and quality assessed by Bioanalyzer. Twenty-five percent of the whole-transcriptome material was processed through v3 library construction according to the manufacturer's protocol. The resulting libraries were quality assessed and quantified again by BioAnalyzer. Libraries were then pooled and sequenced on one lane of a NovaSeq 6000 (S1 100).

Single-cell data analysis—Sequenced samples were initially processed using CellRanger software version 3.0.2 (10x Genomics) and were aligned to the GRCh38 (hg38) human reference genome. CellRanger digital expression matrices (DGE) were generated containing the raw unique molecular identified (UMI) counts for each sample. Count tables were then loaded into R and analyzed using the Seurat package. All cells with fewer than 300 genes or more than 10,000 genes or mitochondrial reads >30% were excluded using Seurat's subset function. Using these parameters, we were able to keep 29,515 cells for downstream analysis. For each cell, UMI counts were log normalized and scaled. Cells were then clustered based on the top 3,000 variable genes identified using the FindVariableFeatures function. Variable genes were then used to perform principal components (PC) analysis, and the first 15 PCs were used for both AD and CTL cells. We then identified clusters using the FindClusters tool and visualized clusters using the uniform manifold approximation and projection (UMAP) dimensionality reduction. Marker genes for each cluster were identified using the FindMarkers function using default parameters.

For monocle analysis, cellranger processed UMIs were imported using the load_cellranger_data function, combined, preprocessed using the preprocess_cds function (num dim = 100), and dimensionality reduced using UMAP with the reduce_dimensions fuction. Cells were then clustered using cluster_cells (resolution = 1e-5). To assess differentiation of fibroblasts to iNs, trajectory analysis was performed using the learn_graph tool. Differential expression analysis between clusters, disease status, or other metadata was performed using graph_test (knn neighbor graph) followed by fit_models with the relevant formula (eg ~ Disease + Patient, etc). Residues from the differential expression were then obtained with the coefficient_table function. Genes with a min expression >0.1 in the iN cluster were used to order cells in pseudotime, and the root node was selected programmatically by first grouping the cells according to which trajectory graph node they were nearest to, calculating the fraction of cells at each node from the earliest time point, and then picking the node that was most heavily occupied by early cells and returning that node as a root. The function plot_genes_in_pseudotime was then used to interrogate how specific genes behaved along pseudotime.

Senescence scoring was done using the AddModuleScore in Seurat, taking the average expression of senescence genes in R-HSA-2559583 subtracted by the aggregate expression of a randomly selected set of control feature sets (n = 100). All analyzed features were binned based on averaged expression, and the control features were randomly selected from each bin.

Telomere length estimation—DNA for telomere estimation was extracted from bulk fibroblast using the DNEasy Blood and Tissue kit (Qiagen). Concentrations were measured via qubit and all samples were diluted to 5ng/uL. Telomere length was assessed via a qPCR strategy as described previously (O'Callaghan 2011). All oligomers used were HPLC purified, and a standard curve was obtained using an 84mer oligonucleotide containing only the TTAGGG repeat. The gene 36B4 was selected as a single copy gene standard to control for genome abundance between samples. All qPCR was performed with SYBR green (Life Technologies) on a BioRad CFX384 thermocycler.

Genome-wide DNA methylation analysis—Genomic DNA was extracted from flow cytometry-isolated iNs or bulk fibroblast cultures using the DNEasy Blood and Tissue Kit (Qiagen). DNA methylation assays were performed on the Illumina MethylEPIC BeadChip as per the standard manufacturers protocol. Raw IDAT files were processed and analyzed in R using the ChAMP and RnBeads packages and were normalized using the BMIQ procedure. Beta values were used as methylation residues for downstream analysis and correlation with RNAseq datasets.

Whole genome assay for transposase-accessible chromatin using sequencing (ATACseq) and analysis—ATAC-Seq was performed as described earlier (Buenrosto 2013). Briefly, 50,000 iNs were lysed in 50 ul lysis buffer (10 mM Tris-HCl ph 7.5, 10 mM NaCl, 3 mM MgCl2, 0.1% IGEPAL, CA-630, in water), pelleted and resuspended in 50 μL transposase reaction mix (1x Tagment DNA buffer, 2.5 μL Tagment DNA enzyme I in water (Illumina)), and incubated at 37°C for 30 min. DNA was purified with Zymo ChIP DNA concentrator columns (Zymo Research). DNA was then amplified with PCR mix (1.25 μM Nextera primer 1, 1.25 μM Nextera primer 2-bar code, 0.6x SYBR Green I (Life Technologies, S7563), 1x NEBNext High-Fidelity 2x PCR MasterMix, (NEBM0541) for 7–10 cycles, run on an agarose gel for size selection of fragments (160–500 bp), and extracted from the gel and paired-end 75 bp sequencing using the Illumina NextSeq 500 platform. Reads were trimmed using TrimGalore and mapped to the UCSC genome build hg38 using STAR. Peaks were then calculated and annotated using the HOMER software package. For agnostic genome-wide characterization of the peaks, sequence depth-normalized bigWig files were used for generating chromatin accessibility profiles using deepTools software. Next, differential accessibility analysis of all identified ATAC-Seq peaks was performed using differential peaks function in HOMER, and fold changes and significance of the resulting differential peaks were plotted as volcano plot using R ggplot2. Genome-wide integration of the ATAC-Seq data with the RNA-Seq data on a gene-by-gene level was performed based on comparing the fold changes of differentially accessible peaks (HOMER differential ATAC peaks) with the fold changes of differentially expressed genes (RNA-Seq expression), using R, and visualization was performed using R ggplot2 and GraphPad Prism software. GSEA of annotated Promoter-TSS peaks was performed using STRING, and overlapping with the Riessland et al. dataset was performed using shared GO terms and enrichment scores present in both datasets. Motif enrichment analysis was performed in HOMER. Statistical enrichment of motifs was performed by using all control iNs as background for AD iN peak and subsequent motif calling. The resulting q-values generated through this method are marked in the figures. Comparisons of peak height between AD and CTL iNs was performed in deeptools using the plotHeatmap function.

ProteinSimple analysis—ProteinSimple Jess (biotechne) was used for low-input digital capillary Western blot-like protein analysis. FACS-purified iNs were plated on Geltrex-coated wells and harvested with PBS. Pellets were then resuspended in RIPA Lysis and Extraction Buffer (Thermo Fisher) containing the cOmplete EDTA-free Protease Inhibitor Cocktail and PhosSTOP phosphatase inhibitors (Sigma Aldrich). Samples were pooled from 9 CTL and AD lines and analyzed using the 12–230 kDa Jess Separation Module. Concentrations of primary antibodies (CDKN2A 1:100) were adjusted to the technology. All

assays were run using the standard default settings provided by ProteinSimple Inc., with the exception of an increased 60-min incubation time for the primary antibodies. Data analysis was performed using Compass software (biotechne).

QUANTIFICATION AND STATISTICAL ANALYSIS

Statistical tests for NGS datasets were performed using built in normalization and significance correction tools in R, GSEA, STRING, HOMER, DESeq2, and deepTools, Seurat, Monocle, and RnBeads. Adjusted p values (padj) indicate that values were corrected for multiple testing using false discovery rates (FDR). Non-omics quantitative data statistics were calculated using GraphPad Prism software with the method indicated for each figure or methods section; for control versus AD comparisons, unpaired t tests and ANOVAs were used. Significance evaluations are marked as *$p < 0.05$; **$p < 0.01$; ***$p < 0.001$; and ****$p < 0.0001$ in the figures.

Supplementary Material

Refer to Web version on PubMed Central for supplementary material.

ACKNOWLEDGMENTS

We are grateful to all donors participating in this study. Special thanks to Gage lab members Raffaella Lucciola, Jeff Jones, Elisa Gorostieta-Salas, M.L. Gage, and Simon Schafer for editorial support. This work was supported by the BrightFocus Foundation (A2019562S); the European Union (EU) grants ERC-STG-2019-852086 and H2020-MSCA-IF-2017-797205; National Institute on Aging grant K99-AG056679; the Chen Foundation; Austrian Science Fund grant FWF-I5057, Clene Nanomedicine; the U.S. National Academy of Medicine (NAM) and the Michael J. Fox Foundation (MJFF) (J.M.); the National Institute on Aging R01 grants AG056306 (J.M and F.H.G.), AG05611, AG057706, and AG072502; the National Institute on Aging P01 grant AG051449; the NIH Training in the Neuroplasticity of Aging grant 5T32AG000216-22; the AHA-Allen Initiative in Brain Health and Cognitive Impairment award made jointly through the American Heart Association and The Paul G. Allen Frontiers Group: 19PABH134610000; Grace Foundation; JPB Foundation; Annette C. Merle-Smith; Lynn and Edward Streim and the Ray and Dagmar Dolby Family Fund; the Milky Way Research Foundation; the Paul G. Allen Family Foundation; Stichting ASC Academy; California Institute for Regenerative Medicine (CIRM) grant RT2-01927 (F.H.G.); the Austrian Marshall Plan Foundation, the L'oreal Austria/ÖUK/ÖAW Stipend; the Theodor Körner Fonds; and the Shiley-Marcos Alzheimer's Disease Research Center (ADRC; AG062429) at the University of California, San Diego (UCSD); the Waitt Advanced Biophotonics Core Facility of the Salk Institute with funding from NIH-NCI CCSG: P30 014195 and the Waitt Foundation; the Flow Cytometry Core Facility of the Salk Institute with funding from NIH-NCI CCSG: P30 014195 and Shared Instrumentation Grant S10-OD023689 (Aria Fusion cell sorter); the NGS Core Facility of the Salk Institute with funding from NIH-NCI CCSG: P30 014195, the Chapman Foundation; and the Stem Cell Core Facility of the Salk Institute.

REFERENCES

1. Mattson MP, and Magnus T (2006). Ageing and neuronal vulnerability. Nat. Rev. Neurosci 7, 278–294. 10.1038/nrn1886. [PubMed: 16552414]
2. Reid DA, Reed PJ, Schlachetzki JCM, Nitulescu II, Chou G, Tsui EC, Jones JR, Chandran S, Lu AT, McClain CA, et al. (2021). Incorporation of a nucleoside analog maps genome repair sites in postmitotic human neurons. Science 372, 91–94. 10.1126/science.abb9032. [PubMed: 33795458]
3. McHugh D, and Gil J (2018). Senescence and aging: Causes, consequences, and therapeutic avenues. J. Cell Biol 217, 65–77. 10.1083/jcb.201708092. [PubMed: 29114066]
4. Farr JN, Fraser DG, Wang H, Jaehn K, Ogrodnik MB, Weivoda MM, Drake MT, Tchkonia T, LeBrasseur NK, Kirkland JL, et al. (2016). Identification of Senescent Cells in the Bone Microenvironment. J. Bone Miner. Res 31, 1920–1929. 10.1002/jbmr.2892. [PubMed: 27341653]

5. Minamino T, Orimo M, Shimizu I, Kunieda T, Yokoyama M, Ito T, Nojima A, Nabetani A, Oike Y, Matsubara H, et al. (2009). A crucial role for adipose tissue p53 in the regulation of insulin resistance. Nat Med 15, 1082–1087. 10.1038/nm.2014. [PubMed: 19718037]
6. Paramos-de-Carvalho D, Martins I, Cristóvão AM, Dias AF, Neves-Silva D, Pereira T, Chapela D, Farinho A, Jacinto A, and Saúde L (2021). Targeting senescent cells improves functional recovery after spinal cord injury. Cell Rep. 36, 109334. 10.1016/j.celrep.2021.109334. [PubMed: 34233184]
7. Sapieha P, and Mallette FA (2018). Cellular Senescence in Postmitotic Cells: Beyond Growth Arrest. Trends Cell Biol. 28, 595–607. 10.1016/j.tcb.2018.03.003. [PubMed: 29704982]
8. Van Cauwenberghe C, Van Broeckhoven C, and Sleegers K (2016). The genetic landscape of Alzheimer disease: clinical implications and perspectives. Genet. Med 18, 421–430. 10.1038/gim.2015.117. [PubMed: 26312828]
9. Lars Rödel TA, Gärtner U, Holzer M, and Holzer M (1996). Expression of the cyclin-dependent kinase inhibitor p16 in Alzheimer's disease. Neuroreport 7, 3047–3050. 10.1097/00001756-199611250-00050. [PubMed: 9116237]
10. McShea A, Harris PL, Webster KR, Wahl AF, and Smith MA (1997). Abnormal expression of the cell cycle regulators P16 and CDK4 in Alzheimer's disease. Am. J. Pathol 150, 1933–1939. [PubMed: 9176387]
11. Rayess H, Wang MB, and Srivatsan ES (2012). Cellular senescence and tumor suppressor gene p16. Int. J. Cancer 130, 1715–1725. 10.1002/ijc.27316. [PubMed: 22025288]
12. Miller JA, Guillozet-Bongaarts A, Gibbons LE, Postupna N, Renz A, Beller AE, Sunkin SM, Ng L, Rose SE, Smith KA, et al. (2017). Neuropathological and transcriptomic characteristics of the aged brain. Elife 6, e31126. 10.7554/eLife.31126. [PubMed: 29120328]
13. Moreno-Blas D, Gorostieta-Salas E, Pommer-Alba A, Mucirño-Hernández G, Gerónimo-Olvera C, Maciel-Barón LA, Konigsberg M, Massieu L, and Castro-Obregón S (2019). Cortical neurons develop a senescence-like phenotype promoted by dysfunctional autophagy. Aging (Albany NY) 11, 6175–6198. 10.18632/aging.102181. [PubMed: 31469660]
14. Jurk D, Wang C, Miwa S, Maddick M, Korolchuk V, Tsolou A, Gonos ES, Thrasivoulou C, Jill Saffrey M, Cameron K, and von Zglinicki T (2012). Postmitotic neurons develop a p21-dependent senescence-like phenotype driven by a DNA damage response. Aging Cell 11, 996–1004. 10.1111/j.1474-9726.2012.00870.x. [PubMed: 22882466]
15. Dehkordi SK, Walker J, Sah E, Bennett E, Atrian F, Frost B, Woost B, Bennett RE, Orr TC, Zhou Y, et al. (2021). Profiling senescent cells in human brains reveals neurons with CDKN2D/p19 and tau neuropathology. Nature Aging 1, 1107–1116. 10.1038/s43587-021-00142-3. [PubMed: 35531351]
16. da Silva PFL, Ogrodnik M, Kucheryavenko O, Glibert J, Miwa S, Cameron K, Ishaq A, Saretzki G, Nagaraja-Grellscheid S, Nelson G , and von Zglinicki T (2019). The bystander effect contributes to the accumulation of senescent cells in vivo. Aging Cell 18, e12848. 10.1111/acel.12848. [PubMed: 30462359]
17. Andrey P, Kiêu K, Kress C, Lehmann G, Tirichine L, Liu Z, Biot E, Adenot PG, Hue-Beauvais C, Houba-Hérin N, et al. (2010). Statistical analysis of 3D images detects regular spatial distributions of centromeres and chromocenters in animal and plant nuclei. PLoS Comput. Biol 6, e1000853. 10.1371/journal.pcbi.1000853. [PubMed: 20628576]
18. Herdy J, Schafer S, Kim Y, Ansari Z, Zangwill D, Ku M, Paquola A, Lee H, Mertens J, and Gage FH (2019). Chemical modulation of transcriptionally enriched signaling pathways to optimize the conversion of fibroblasts into neurons. Elife 8, e41356. 10.7554/eLife.41356. [PubMed: 31099332]
19. Mertens J, Paquola AC, Ku M, Hatch E, Böhnke L, Ladjevardi S, McGrath S, Campbell B, Lee H, Herdy JR, et al. (2015). Directly Reprogrammed Human Neurons Retain Aging-Associated Transcriptomic Signatures and Reveal Age-Related Nucleocytoplasmic Defects. Cell Stem Cell 17, 705–718. 10.1016/j.stem.2015.09.001. [PubMed: 26456686]
20. Kim Y, Zheng X, Ansari Z, Bunnell MC, Herdy JR, Traxler L, Lee H, Paquola AC, Blithikioti C, Ku M, et al. (2018). Mitochondrial Aging Defects Emerge in Directly Reprogrammed Human Neurons due to Their Metabolic Profile. Cell Rep. 23, 2550–2558. 10.1016/j.cel-rep.2018.04.105. [PubMed: 29847787]

21. Mertens J, Herdy JR, Traxler L, Schafer ST, Schlachetzki JC, Böhnke L, Reid DA, Lee H, Zangwill D, Fernandes DP, et al. (2021). Age-dependent instability of mature neuronal fate in induced neurons from Alzheimer's patients. Cell Stem Cell 28, 1533–1548.e6. e1536. 10.1016/j.stem.2021.04.004. [PubMed: 33910058]
22. Huh CJ, Zhang B, Victor MB, Dahiya S, Batista LF, Horvath S, and Yoo AS (2016). Maintenance of age in human neurons generated by microRNA-based neuronal conversion of fibroblasts. Elife 5, e18648. 10.7554/eLife.18648. [PubMed: 27644593]
23. Victor MB, Richner M, Olsen HE, Lee SW, Monteys AM, Ma C, Huh CJ, Zhang B, Davidson BL, Yang XW, and Yoo AS (2018). Striatal neurons directly converted from Huntington's disease patient fibroblasts recapitulate age-associated disease phenotypes. Nat. Neurosci 21, 341–352. 10.1038/s41593-018-0075-7. [PubMed: 29403030]
24. Tang Y, Xiong S, Yu P, Liu F, and Cheng L (2018). Direct Conversion of Mouse Fibroblasts into Neural Stem Cells by Chemical Cocktail Requires Stepwise Activation of Growth Factors and Nup210. Cell Rep. 24, 1355–1362.e3. e1353. 10.1016/j.celrep.2018.06.116. [PubMed: 30067988]
25. Ladewig J, Mertens J, Kesavan J, Doerr J, Poppe D, Glaue F, Herms S, Wernet P, Kögler G, Müller FJ, et al. (2012). Small molecules enable highly efficient neuronal conversion of human fibroblasts. Nat. Methods 9, 575–578. 10.1038/nmeth.1972. [PubMed: 22484851]
26. Vadodaria KC, Mertens J, Paquola A, Bardy C, Li X, Jappelli R, Fung L, Marchetto MC, Hamm M, Gorris M, et al. (2016). Generation of functional human serotonergic neurons from fibroblasts. Mol Psychiatry 21, 49–61. 10.1038/mp.2015.161. [PubMed: 26503761]
27. Mertens J, Reid D, Lau S, Kim Y, and Gage FH (2018). Aging in a Dish: iPSC-Derived and Directly Induced Neurons for Studying Brain Aging and Age-Related Neurodegenerative Diseases. Annu. Rev. Genet 52, 271–293. 10.1146/annurev-genet-120417-031534. [PubMed: 30208291]
28. Handel AE, Chintawar S, Lalic T, Whiteley E, Vowles J, Giustacchini A, Argoud K, Sopp P, Nakanishi M, Bowden R, et al. (2016). Assessing similarity to primary tissue and cortical layer identity in induced pluripotent stem cell-derived cortical neurons through single-cell transcriptomics. Hum. Mol. Genet 25, 989–1000. 10.1093/hmg/ddv637. [PubMed: 26740550]
29. Coppé JP, Desprez PY, Krtolica A, and Campisi J (2010). The senescence-associated secretory phenotype: the dark side of tumor suppression. Annu. Rev. Pathol 5, 99–118. 10.1146/annurev-pathol-121808-102144. [PubMed: 20078217]
30. Chen JL, Margolis DJ, Stankov A, Sumanovski LT, Schneider BL, and Helmchen F (2015). Pathway-specific reorganization of projection neurons in somatosensory cortex during learning. Nat. Neurosci 18, 1101–1108. 10.1038/nn.4046. [PubMed: 26098757]
31. Usardi A, Iyer K, Sigoillot SM, Dusonchet A, and Selimi F (2017).The immunoglobulin-like superfamily member IGSF3 is a developmentally regulated protein that controls neuronal morphogenesis. Dev Neurobiol 77, 75–92. 10.1002/dneu.22412. [PubMed: 27328461]
32. Riessland M, Kolisnyk B, Kim TW, Cheng J, Ni J, Pearson JA, Park EJ, Dam K, Acehan D, Ramos-Espiritu LS, et al. (2019). Loss of SATB1 Induces p21-Dependent Cellular Senescence in Post-mitotic Dopaminergic Neurons. Cell Stem Cell 25, 514–530.e8. e518. 10.1016/j.stem.2019.08.013. [PubMed: 31543366]
33. Moore LD, Le T, and Fan G (2013). DNA methylation and its basic function. Neuropsychopharmacology 38, 23–38. 10.1038/npp.2012.112. [PubMed: 22781841]
34. Contrepois K, Coudereau C, Benayoun BA, Schuler N, Roux PF, Bischof O, Courbeyrette R, Carvalho C, Thuret JY, Ma Z, et al. (2017). Histone variant H2A.J accumulates in senescent cells and promotes inflammatory gene expression. Nat. Commun 8, 14995. 10.1038/ncomms14995. [PubMed: 28489069]
35. Ohtani N, Zebedee Z, Huot TJG, Stinson JA, Sugimoto M, Ohashi Y, Sharrocks AD, Peters G, and Hara E (2001). Opposing effects of Ets and Id proteins on p16INK4a expression during cellular senescence. Nature 409, 1067–1070. 10.1038/35059131. [PubMed: 11234019]
36. Hänzelmann S, Beier F, Gusmao EG, Koch CM, Hummel S, Charapitsa I, Joussen S, Benes V, Brümmendorf TH, Reid G, et al. (2015). Replicative senescence is associated with nuclear reorganization and with DNA methylation at specific transcription factor binding sites. Clin Epigenetics 7, 19. 10.1186/s13148-015-0057-5. [PubMed: 25763115]

37. Cawthon RM (2002). Telomere measurement by quantitative PCR. Nucleic Acids Res. 30. e47–47. 10.1093/nar/30.10.e47. [PubMed: 12000852]
38. O'Callaghan NJ, Dhillon VS, Thomas P, and Fenech M (2008). A quantitative real-time PCR method for absolute telomere length. Biotechniques 44, 807–809. 10.2144/000112761. [PubMed: 18476834]
39. Koch CM, and Wagner W (2013). Epigenetic biomarker to determine replicative senescence of cultured cells. Methods Mol. Biol 1048, 309–321. 10.1007/978-1-62703-556-9_20. [PubMed: 23929112]
40. Denchi EL, and de Lange T (2007). Protection of telomeres through independent control of ATM and ATR by TRF2 and POT1. Nature 448, 1068–1071. 10.1038/nature06065. [PubMed: 17687332]
41. Chow HM, Shi M, Cheng A, Gao Y, Chen G, Song X, So RWL, Zhang J, and Herrup K (2019). Age-related hyperinsulinemia leads to insulin resistance in neurons and cell-cycle-induced senescence. Nat. Neurosci 22, 1806–1819. 10.1038/s41593-019-0505-1. [PubMed: 31636448]
42. Cao J, Spielmann M, Qiu X, Huang X, Ibrahim DM, Hill AJ, Zhang F, Mundlos S, Christiansen L, Steemers FJ, et al. (2019). The single-cell transcriptional landscape of mammalian organogenesis. Nature 566, 496–502. 10.1038/s41586-019-0969-x. [PubMed: 30787437]
43. Coppe JP, Desprez PY, Krtolica A, and Campisi J (2010). The senescence-associated secretory phenotype: the dark side of tumor suppression. Annu. Rev. Pathol 5, 99–118. 10.1146/annurev-pathol-121808-102144. [PubMed: 20078217]
44. Stein GH, Drullinger LF, Soulard A, and Dulić V (1999). Differential roles for cyclin-dependent kinase inhibitors p21 and p16 in the mechanisms of senescence and differentiation in human fibroblasts. Mol. Cell Biol 19, 2109–2117. 10.1128/MCB.19.3.2109. [PubMed: 10022898]
45. Morabito S, Miyoshi E, Michael N, Shahin S, Martini AC, Head E, Silva J, Leavy K, Perez-Rosendahl M, and Swarup V (2021). Singlenucleus chromatin accessibility and transcriptomic characterization of Alzheimer's disease. Nat. Genet 53, 1143–1155. 10.1038/s41588-021-00894-z. [PubMed: 34239132]
46. Rodríguez JJ, Olabarria M, Chvatal A, and Verkhratsky A (2009). Astroglia in dementia and Alzheimer's disease. Cell Death Differ. 16, 378–385. 10.1038/cdd.2008.172. [PubMed: 19057621]
47. Basisty N, Kale A, Jeon OH, Kuehnemann C, Payne T, Rao C, Holtz A, Shah S, Sharma V, Ferrucci L, et al. (2020). A proteomic atlas of senescence-associated secretomes for aging biomarker development. PLoS Biol. 18, e3000599. 10.1371/journal.pbio.3000599. [PubMed: 31945054]
48. Hill LJ, Di Pietro V, Hazeldine J, Davies D, Toman E, Logan A, and Belli A (2018). Author Correction: Cystatin D (CST5): An ultra-early inflammatory biomarker of traumatic brain injury. Sci. Rep 8, 4572. 10.1038/s41598-018-22951-0. [PubMed: 29531266]
49. Whelan CD, Mattsson N, Nagle MW, Vijayaraghavan S, Hyde C, Janelidze S, Stomrud E, Lee J, Fitz L, Samad TA, et al. (2019). Multiplex proteomics identifies novel CSF and plasma biomarkers of early Alzheimer's disease. Acta Neuropathol Commun 7, 169. 10.1186/s40478-019-0795-2. [PubMed: 31694701]
50. Escartin C, Galea E, Lakatos A, O'Callaghan JP, Petzold GC, Serrano-Pozo A, Steinhäuser C, Volterra A, Carmignoto G, Agarwal A, et al. (2021). Reactive astrocyte nomenclature, definitions, and future directions. Nat. Neurosci 24, 312–325. 10.1038/s41593-020-00783-4. [PubMed: 33589835]
51. Visse R, and Nagase H (2003). Matrix metalloproteinases and tissue inhibitors of metalloproteinases: structure, function, and biochemistry. Circ. Res 92, 827–839. 10.1161/01.RES.0000070112.80711.3D. [PubMed: 12730128]
52. Mathys H, Davila-Velderrain J, Peng Z, Gao F, Mohammadi S, Young JZ, Menon M, He L, Abdurrob F, Jiang X, et al. (2019). Single-cell transcriptomic analysis of Alzheimer's disease. Nature 570, 332–337. 10.1038/s41586-019-1195-2. [PubMed: 31042697]
53. Limbad C, Oron TR, Alimirah F, Davalos AR, Tracy TE, Gan L, Desprez PY, and Campisi J (2020). Astrocyte senescence promotes glutamate toxicity in cortical neurons. PLoS One 15, e0227887. 10.1371/journal.pone.0227887. [PubMed: 31945125]

54. Yaswen P, and Campisi J (2007). Oncogene-induced senescence pathways weave an intricate tapestry. Cell 128, 233–234. 10.1016/j.cell.2007.01.005. [PubMed: 17254959]
55. Collado M, and Serrano M (2010). Senescence in tumours: evidence from mice and humans. Nat. Rev. Cancer 10, 51–57. 10.1038/nrc2772. [PubMed: 20029423]
56. Bartkova J, Rezaei N, Liontos M, Karakaidos P, Kletsas D, Issaeva N, Vassiliou LVF, Kolettas E, Niforou K, Zoumpourlis VC, et al. (2006). Oncogene-induced senescence is part of the tumorigenesis barrier imposed by DNA damage checkpoints. Nature 444, 633–637. 10.1038/nature05268. [PubMed: 17136093]
57. Bussian TJ, Aziz A, Meyer CF, Swenson BL, van Deursen JM, and Baker DJ (2018). Clearance of senescent glial cells prevents tau-dependent pathology and cognitive decline. Nature 562, 578–582. 10.1038/s41586-018-0543-y. [PubMed: 30232451]
58. Musi N, Valentine JM, Sickora KR, Baeuerle E, Thompson CS, Shen Q, and Orr ME (2018). Tau protein aggregation is associated with cellular senescence in the brain. Aging Cell 17, e12840. 10.1111/acel.12840. [PubMed: 30126037]
59. Zhang P, Kishimoto Y, Grammatikakis I, Gottimukkala K, Cutler RG, Zhang S, Abdelmohsen K, Bohr VA, Misra Sen J, Gorospe M, and Mattson MP (2019). Senolytic therapy alleviates Aβ-associated oligodendrocyte progenitor cell senescence and cognitive deficits in an Alzheimer's disease model. Nat. Neurosci 22, 719–728. 10.1038/s41593-019-0372-9. [PubMed: 30936558]
60. Ogrodnik M, Evans SA, Fielder E, Victorelli S, Kruger P, Salmonowicz H, Weigand BM, Patel AD, Pirtskhalava T, Inman CL, et al. (2021). Whole-body senescent cell clearance alleviates age-related brain inflammation and cognitive impairment in mice. Aging Cell 20, e13296. 10.1111/acel.13296. [PubMed: 33470505]
61. McConnell BB, Starborg M, Brookes S, and Peters G (1998). Inhibitors of cyclin-dependent kinases induce features of replicative senescence in early passage human diploid fibroblasts. Curr. Biol 8, 351–354. 10.1016/s0960-9822(98)70137-x. [PubMed: 9512419]
62. Azazmeh N, Assouline B, Winter E, Ruppo S, Nevo Y, Maly A, Meir K, Witkiewicz AK, Cohen J, Rizou SV, et al. (2020). Chronic expression of p16INK4a in the epidermis induces Wnt-mediated hyperplasia and promotes tumor initiation. Nat. Commun. 11, 2711. 10.1038/s41467-020-16475-3. [PubMed: 32483135]
63. Storer M, Mas A, Robert-Moreno A, Pecoraro M, Ortells M, Di Giacomo V, Yosef R, Pilpel N, Krizhanovsky V, Sharpe J, and Keyes W (2013). Senescence is a developmental mechanism that contributes to embryonic growth and patterning. Cell 155, 1119–1130. 10.1016/j.cell.2013.10.041. [PubMed: 24238961]
64. Demaria M, Ohtani N, Youssef S, Rodier F, Toussaint W, Mitchell J, Laberge RM, Vijg J, Van Steeg H, Dollé M, et al. (2014). An essential role for senescent cells in optimal wound healing through secretion of PDGF-AA. Dev. Cell 31, 722–733. 10.1016/j.devcel.2014.11.012. [PubMed: 25499914]
65. Mederos S, González-Arias C, and Perea G (2018). Astrocyte-Neuron Networks: A Multilane Highway of Signaling for Homeostatic Brain Function. Front. Synaptic Neurosci 10, 45. 10.3389/fnsyn.2018.00045. [PubMed: 30542276]
66. González-Gualda E, Baker AG, Fruk L, and Muñoz-Espín D (2021). A guide to assessing cellular senescence in vitro and in vivo. FEBS J. 288, 56–80. 10.1111/febs.15570. [PubMed: 32961620]
67. Welch GM, Boix CA, Schmauch E, Davila-Velderrain J, Victor MB, Dileep V, Bozzelli PL, Su Q, Cheng JD, Lee A, et al. (2022). Neurons burdened by DNA double-strand breaks incite microglia activation through antiviral-like signaling in neurodegeneration. Sci. Adv 8, eabo4662. 10.1126/sciadv.abo4662. [PubMed: 36170369]
68. Han X, Zhang T, Liu H, Mi Y, and Gou X (2020). Astrocyte Senescence and Alzheimer's Disease: A Review. Front. Aging Neurosci 12, 148. 10.3389/fnagi.2020.00148. [PubMed: 32581763]
69. Gillispie GJ, Sah E, Krishnamurthy S, Ahmidouch MY, Zhang B, and Orr ME (2021). Evidence of the Cellular Senescence Stress Response in Mitotically Active Brain Cells-Implications for Cancer and Neurodegeneration. Life 11, 153. 10.3390/life11020153. [PubMed: 33671362]
70. Traxler L, Herdy JR, Stefanoni D, Eichhorner S, Pelucchi S, Szücs A, Santagostino A, Kim Y, Agarwal RK, Schlachetzki JC, et al. (2022). Warburg-like metabolic transformation underlies

neuronal degeneration in sporadic Alzheimer's disease. Cell Metab 34, 1248–1263.e6. e1246. 10.1016/j.cmet.2022.07.014. [PubMed: 35987203]

71. Herrup K (2010). The involvement of cell cycle events in the pathogenesis of Alzheimer's disease. Alzheimer's Res. Ther 2, 13. 10.1186/alzrt37. [PubMed: 20497605]
72. Lanni C, Masi M, Racchi M, and Govoni S (2021). Cancer and Alzheimer's disease inverse relationship: an age-associated diverging derailment of shared pathways. Mol Psychiatry 26, 280–295. 10.1038/s41380-020-0760-2. [PubMed: 32382138]
73. Li JM, Liu C, Hu X, Cai Y, Ma C, Luo XG, and Yan XX (2014). Inverse correlation between Alzheimer's disease and cancer: implication for a strong impact of regenerative propensity on neurodegeneration? BMC Neurol. 14, 211. 10.1186/s12883-014-0211-2. [PubMed: 25394409]
74. Wilkinson HN, and Hardman MJ (2020). Senescence in Wound Repair: Emerging Strategies to Target Chronic Healing Wounds. Front. Cell Dev. Biol 8, 773. 10.3389/fcell.2020.00773. [PubMed: 32850866]
75. Buenrostro JD, Giresi PG, Zaba LC, Chang HY, and Greenleaf WJ (2013).Transposition of native chromatin for fast and sensitive epigenomic profiling of open chromatin, DNA-binding proteins and nucleosome position. Nat. Methods 10, 1213–1218. 10.1038/nmeth.2688. [PubMed: 24097267]
76. Schafer ST, Paquola ACM, Stern S, Gosselin D, Ku M, Pena M, Kuret TJM, Liyanage M, Mansour AA, Jaeger BN, et al. (2019). Pathological priming causes developmental gene network heterochronicity in autistic subject-derived neurons. Nat. Neurosci 22, 243–255. 10.1038/s41593-018-0295-x. [PubMed: 30617258]
77. Mertens J, Paquola AC, Ku M, Hatch E, Bohnke L, Ladjevardi S, McGrath S, Campbell B, Lee H, Herdy JR, et al. (2015). Directly Reprogrammed Human Neurons Retain Aging-Associated Transcriptomic Signatures and Reveal Age-Related Nucleocytoplasmic Defects. Cell Stem Cell 17, 705–718. 10.1016/j.stem.2015.09.001. [PubMed: 26456686]
78. Zeng H, Jorapur A, Shain AH, Lang UE, Torres R, Zhang Y, McNeal AS, Botton T, Lin J, Donne M, et al. (2018). Bi-allelic Loss of CDKN2A Initiates Melanoma Invasion via BRN2 Activation. Cancer Cell 34, 56–68.e9. 10.1016/j.ccell.2018.05.014. [PubMed: 29990501]
79. Zhang K, Myllymäki SM, Gao P, Devarajan R, Kytölä V, Nykter M, Wei GH, and Manninen A (2017). Oncogenic K-Ras upregulates ITGA6 expression via FOSL1 to induce anoikis resistance and synergizes with αV-Class integrins to promote EMT. Oncogene 36, 5681–5694. 10.1038/onc.2017.177. [PubMed: 28604746]
80. Israel MA, Yuan SH, Bardy C, Reyna SM, Mu Y, Herrera C, Hefferan MP, Van Gorp S, Nazor KL, Boscolo FS, et al. (2012). Probing sporadic and familial Alzheimer's disease using induced pluripotent stem cells. Nature 482, 216–220. 10.1038/nature10821. [PubMed: 22278060]

Highlights

- Aged, induced neurons (iNs) endogenously present features of cellular senescence
- Alzheimer's neurons senesce more frequently than healthy controls
- Senescent neurons gain an inflammatory senescence-associated secretory phenotype
- Senescent neurons can be eliminated with senotherapeutics

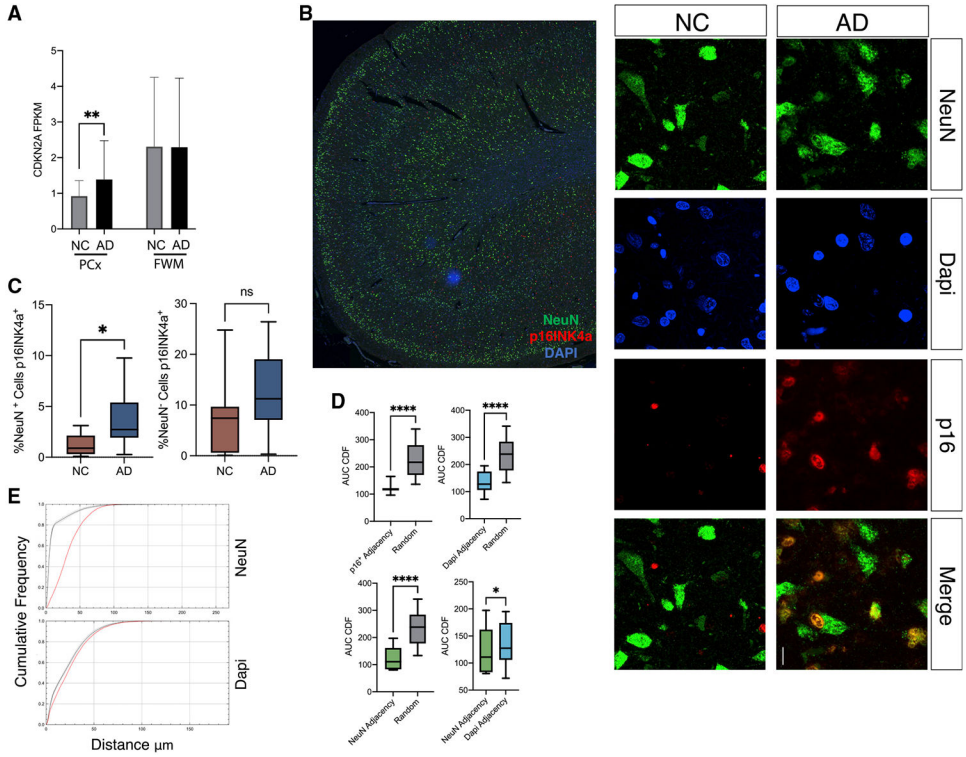

Figure 1. The human AD brain harbors an increased proportion of senescent neurons

(A) Expression of CDKN2A in the brains of Alzheimer's disease (AD) patients and cognitively normal (NC) controls in the pre-frontal cortex (PCx) and frontal white matter (FWM) (Wald test DESeq2, n = AD 30; 99 NC).

(B) Fluorescence microscopy analysis of p16 expression in post-mortem PCx tissue from AD and NC patients, left 20X, right 63X, scale bar = 16 µm.

(C) Quantification of p16 expression in $NeuN^+$ cells (left) and $DAPI^+$ nuclei (right) (n = AD 10; 10 NC, unpaired t test).

(D) Clustering analysis of p16 signal adjacent to other $p16^+$ loci (top left), $DAPI^+$ loci (top right), $NeuN^+$ loci (bottom left), and NeuN adjacency compared with DAPI adjacency (bottom right) (n = AD 10; 10 NC, paired t test).

(E) Example cumulative distribution function for p16 signal near $NeuN^+$ and $DAPI^+$ loci used to calculate the adjacency AUC in (D).

*p < 0.05, **p < 0.01, ****p < 0.0001.

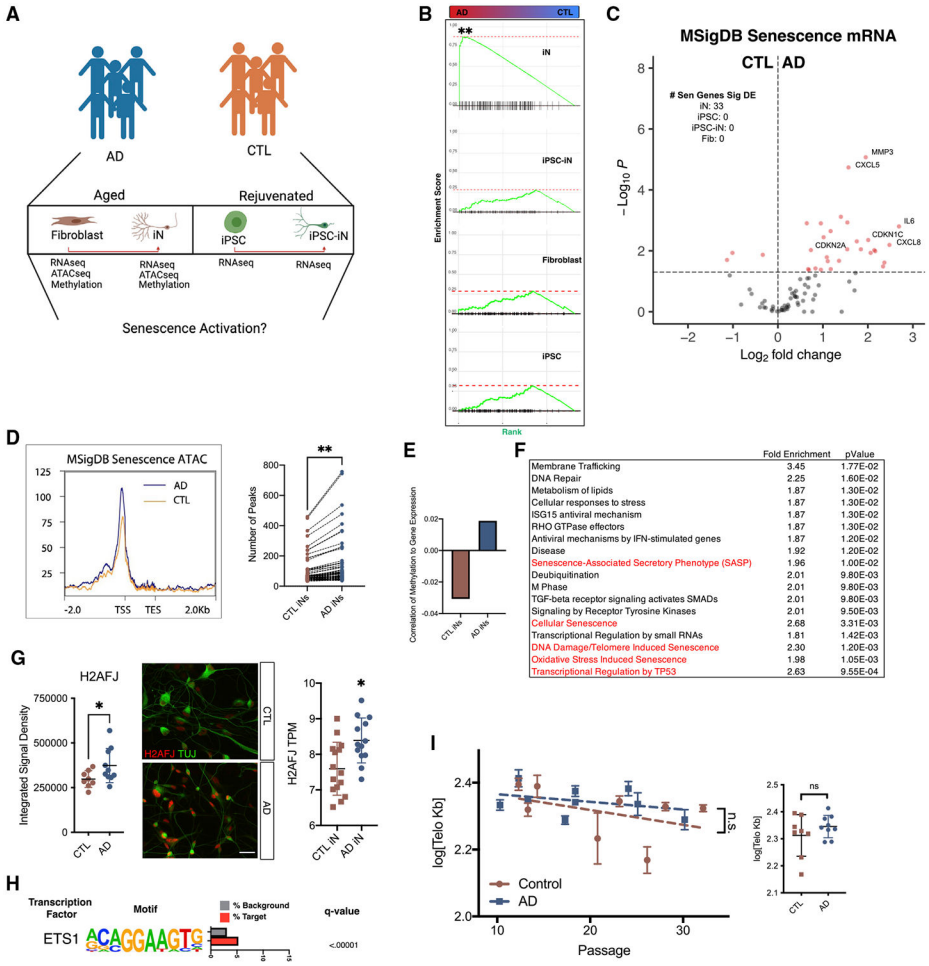

Figure 2. Senescence changes in the transcriptome and epigenome of aged AD neurons

(A) Experimental schema.

(B) GSEA of differential expression of AD and CTL in four cell types: iNs (aged induced neurons n = 35), iPSC-iNs (rejuvenated young neurons, n = 20), iPSCs (n = 20), and fibroblasts (n = 35); indicates a significant enrichment exclusively (q value = 0.012) in AD iNs.

(C) Volcano plot of genes used for GSEA in (B) in iNs. Genes above the significance threshold (padj < 0.05, Log2FC > 1) are colored red.

(D) Histogram of peaks averaged from AD 10 and 10 CTL iN samples across senescence genes, including the transcription start site (TSS) and transcription end site (TES) and 2kb window (left). Peak counts in senescence genes are significantly higher in AD iNs than in CTLs (right); each point represents the number of peaks in a single gene in our senescence gene list (Mann-Whitney test).

(E) Increased promoter methylation is negatively associated with senescence gene expression in CTL iNs and positively associated with expression in AD iNs (n = AD 8; 8 CTL).

(F) GO analysis of genes with low promoter methylation and high expression in AD iNs.

(G) H2AFJ is expressed significantly higher in AD iNs (right) and shows significantly brighter staining by ICC (left); scale bar = 16 μm.

(H) The binding motif for the transcription factor ETS1 is significantly enriched in open chromatin in AD (target) relative to CTL (background) iNs.
(I) There are no significant differences between telomere erosion in AD and CTL parent fibroblast lines or in total telomere content, as measured by qPCR.
*$p < 0.05$, **$p < 0.01$.

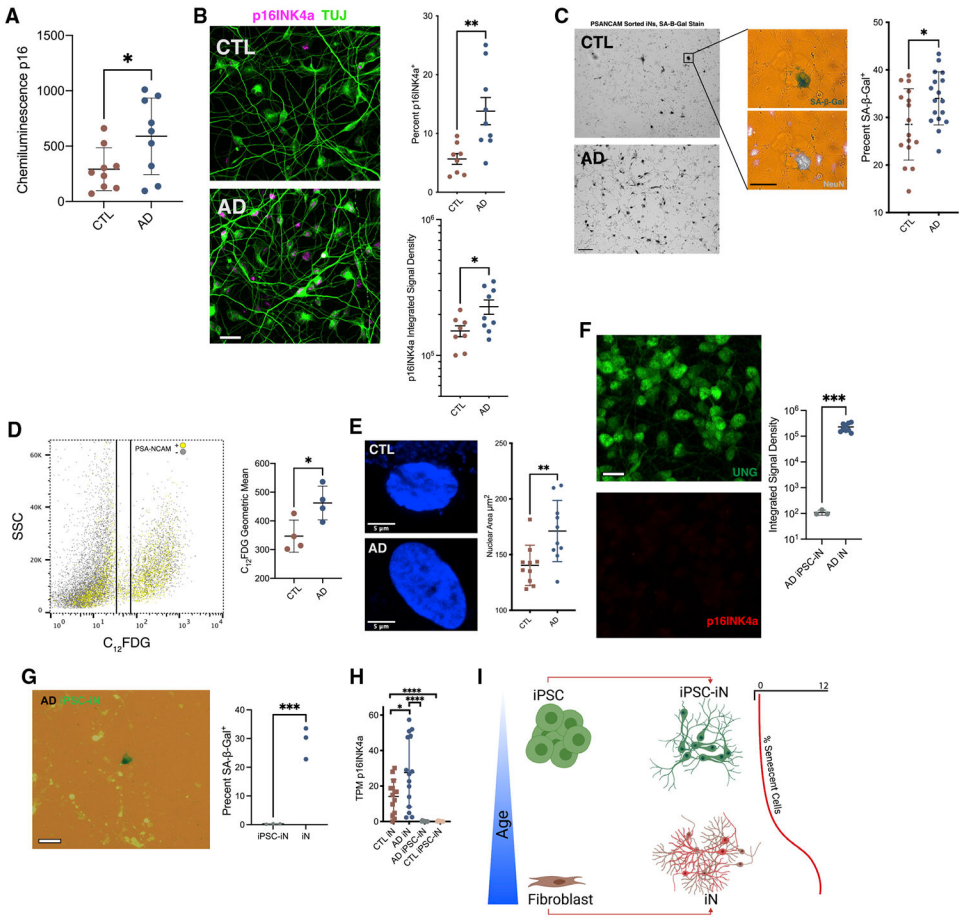

Figure 3. iNs present *bona fide* markers of cellular senescence

(A) AD iNs have increased p16 protein measured by chemiluminescence in a capillary western blot analysis (n = AD 9; 9 CTL, unpaired t test).

(B) Example confocal images of p16 co-stained with Tuj in PSA-NCAM-sorted iNs; scale bar = 16 µm (left). AD iNs have a significantly increased population and intensity of $p16^{+}$ cells (right) (n = AD 9; 8 CTL, unpaired t test).

(C) Example picture of PSANCAM-sorted iNs stained for SA-B-Gal and co-stained for mature neuron marker NeuN (left); scale bar = 8 µm. Quantification of $BGal^{+}$ rates in AD and CTL iN cultures (right) (n = AD 17, 16 CTL, unpaired t test).

(D) Example FACS gating to separate $C12^{+}$ from $C12^{-}$ cells (left). AD iNs have a significantly larger $C12^{+}$ population, as indicated by a higher geometric mean of C12 signal (right) (n = AD 4; 4 CTL, unpaired t test).

(E) Example images of CTL and AD nuclei stained with DAPI (left). AD iNs have increased nuclear area measured by integrated DAPI signal (right) (n = AD 10 and 10 CTL patients, unpaired t test).

(F) Example images of p16 and UNG:GFP in iPSC-derived AD iNs; scale bar = 16 µm (left). Quantification of p16 signal intensity in iPSC-derived AD iNs (right) (n = 3 iPSC-iN; 3 iN, unpaired t test).

(G) Example BGal staining in iPSC-iN cultures; scale bar = 8 µm (left). Quantification of $BGal^{+}$ rates in AD iPSC-iNs or fibroblast iNs (right) (n = 3 iPSC-iN; 3 iN, unpaired t test).

(H) P16ink4a is not expressed in iPSC-iNs.

(I) Senescent-like phenotypes manifest only in aged human neurons, but young rejuvenated iPSC-iNs do not present senescence markers under baseline conditions.

*p < 0.05, **p < 0.01, ***p < 0.001, ****p < 0.0001.

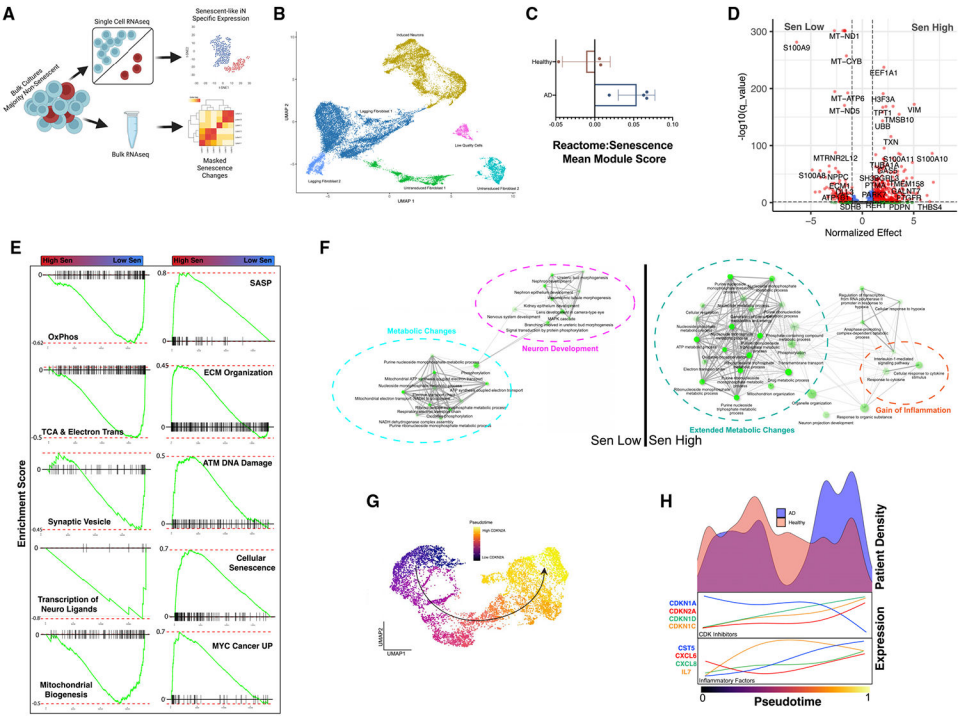

Figure 4. scRNA-seq indicates oncogenic challenges and metabolic dysfunction in senescent neurons

(A) ScRNA-seq allows us to discriminate senescent gene expression from the majority of non-senescent cells that mask expression in bulk RNAseq.

(B) UMAP clustering of all unsorted fibroblast to iN cultures after 3 weeks of conversion from AD 4 and 3 CTL patients.

(C) Mean module score for each patient in iNs.

(D) Volcano plot of genes differentially expressed between sen-low and sen-high iNs.

(E) GSEA of gene sets enriched (right) or depleted (left) in sen-high cells.

(F) Gene network analysis of genes enriched in AD iNs in sen-low (left) or sen-high (right) populations.

(G) UMAP projection of iNs colored by their rank in pseudotime analysis tracking the expression of CDKN2A.

(H) Density plot of patient proportions across CDKN2A pseudotime and gene expression changes across pseudotime.

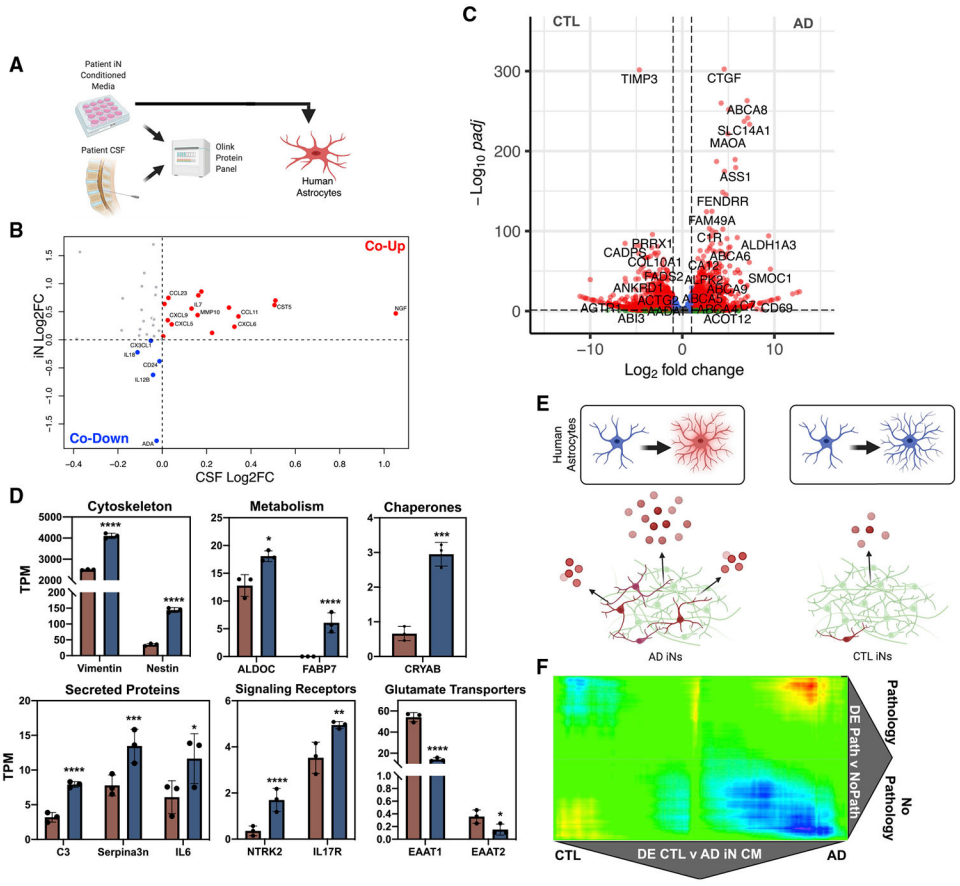

Figure 5. AD-conditioned media triggers reactive astrogliosis

(A) Experimental paradigm. Cerebral spinal fluid (CSF) and patient iN conditioned media (CM) were submitted for a multiplex inflammation panel, and CM was applied to human astrocytes to evaluate reactivity.

(B) Overlap of log2FC of inflammatory probes (AD/CTL) from CSF and iN CM. Co-upregulated in AD in red and co-downregulated in blue.

(C) Differential expression analysis between AD and CTL CM-treated astrocytes reveals 981 genes significantly differentially expressed (n = 3 astrocyte cell lines).

(D) Expression of reactive astrocyte markers in AD- or CTL-treated astrocytes (n = 3, Wald test DESeq2).

(E) A larger population of senescent-like neurons triggered a hyperreactive state in human astrocytes.

(F) RRHO mapping of the transcriptional overlap between astrocytes from post-mortem patients with or without AD pathology and between astrocytes treated with AD or CTL CM *in vitro*.

*p < 0.05, **p < 0.01, ***p < 0.001, ****p < 0.0001.

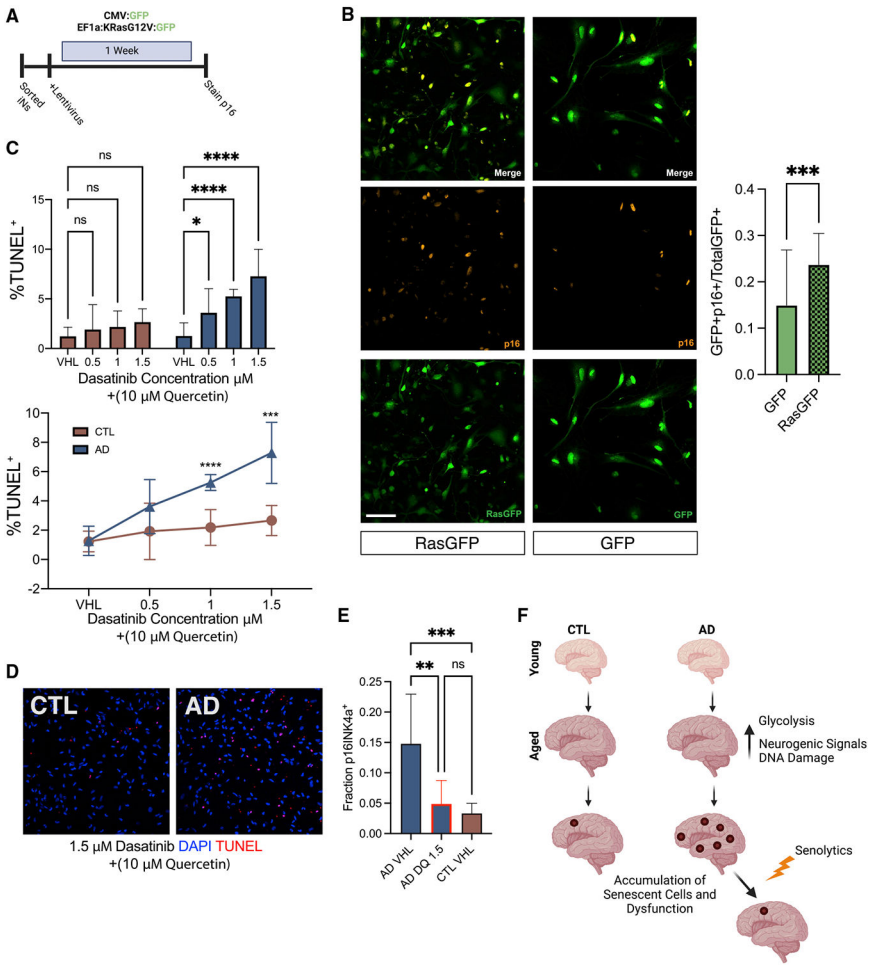

Figure 6. Senescence in neurons can be triggered by oncogenes and eliminated with senotherapeutics

(A) Ras overexpression experimental scheme.

(B) Representative image of Ras- or GFP-treated iNs and p16 staining (left). Ras-treated iNs are significantly more likely to be $p16^+$ than GFP controls (right) (n = 8 biological replicates per condition, paired t test).

(C) AD iN cultures experience a dose-dependent increase in number of $TUNEL^+$ cells after exposure to senolytic cocktail dasatinib +10 µM quercetin (n = AD 3; 3 CTL, two-way ANOVA).

(D) Representative field of iN cultures from AD or CTL patients treated with 1.5 µM dasatinib +10 µM quercetin.

(E) AD cultures have significantly reduced $p16^+$ cells after D + Q treatments that are comparable to CTL p16 levels (n = AD 3; 3 CTL, one-way ANOVA).

(F) Theory cartoon.

*p < 0.05, **p < 0.01, ***p < 0.001, ****p < 0.0001.

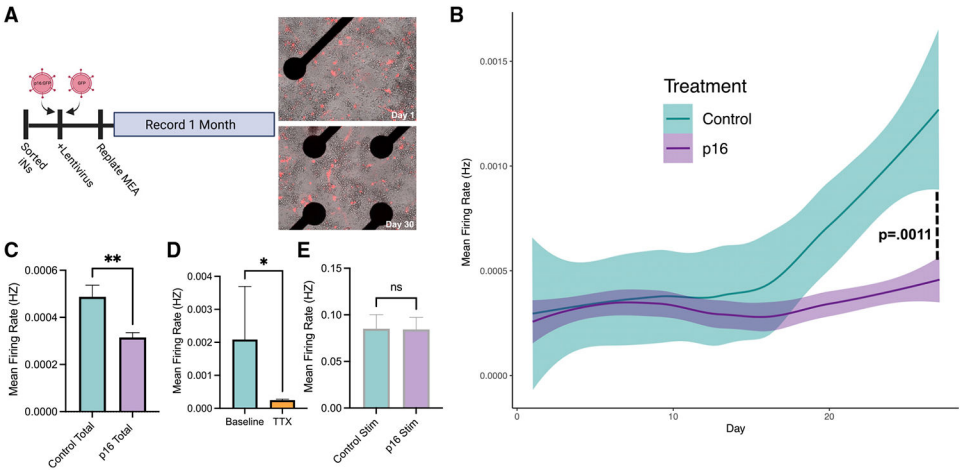

Figure 7. Neuronal senescence manifests in impaired electrical activity

(A) Experimental schema. Sorted iNs were treated with p16 or control lentivirus and cultured on multi electrode array (MEA) plates for one month of recording (left). Example images of synpasin:dsRed-labeled iNs on an MEA plate at 24 h and one month after replating (right).

(B) Ribbon plot of mean firing rate of p16 or GFP iNs. The slope of activity change overtime was significantly higher in GFP than in p16-expressing iNs (n = 18 recording wells for each condition; two-tailed t test).

(C) The cumulative mean firing rate across all 30 days of recording in GFP iNs was significantly higher than p16 iNs. Measurements across all wells were averaged into a single point for a given day (n = 30, paired t test).

(D) Activity of iNs could be ablated with treatment of 1 uM tetrodotoxin (n = 18 recording wells, paired t test).

(E) There were no significant differences in the mean firing rate of GFP and p16 iNs following electrical stimulation (Stim) (n = 18 recording wells for each condition, paired t test).

*p< 0.05, **p< 0.01.

KEY RESOURCES TABLE

REAGENT or RESOURCE	SOURCE	IDENTIFIER
Antibodies		
Mouse anti NeuN	EMD Millipore	Cat# MAB377, RRID:AB_2298772
Rabbit anti p16INK4a	Abcam	Cat# ab108349, RRID:AB_10858268
Goat anti p16INK4a	R&D Systems	Cat# AF5779, RRID:AB_1964666
Mouse anti TuJ	BioLegend	Cat# 801201, RRID:AB_2313773
Rabbit anti GFAP	EMD Millipore	Cat# AB5804, RRID:AB_2109645
Rabbit anti LaminB1	Invitrogen	Cat# MA5-32066. RRID:AB_2809360
Mouse anti PSA-NCAM	Miltenyl Biotec	Cat#130-120-437
Goat anti Vimentin	Millipore	Cat# AB1620, RRID:AB_90774
Alexa Fluor 488-conjugated Donkey Anti Rabbit IgG	Thermo Fisher Scientific	Cat#A-21206
Alexa Fluor 647-conjugated Donkey Anti Rabbit IgG	Thermo Fisher Scientific	Cat#A-31573
Cy3-conjugated Donkey Anti-Rabbit IgG	Jackson ImmunoRes.	Cat#711-165-152
Alexa Fluor 488-conjugated Donkey Anti Mouse IgG	Thermo Fisher Scientific	Cat#A-21202
Alexa Fluor 647-conjugated Donkey Anti Mouse IgG	Thermo Fisher Scientific	Cat#A-31571
Cy3-conjugated Donkey Anti-Mouse IgG	Jackson ImmunoRes.	Cat#711-165-151
Bacterial and virus strains		
NEB Stable Competent *E. coli*	New England Biolabs	Cat#C3040H
Biological samples		
Human Pre-frontal Cortex FFPE Sections	UCSD Shiley-Marcos Alzheimer's Disease Research Center	Table S1
Fibroblast Cultures from Cohort	This study	Table S5
iPSC Cultures from Cohort	This study	Table S5
Chemicals, peptides, and recombinant proteins		
TrypLE	Gibco	Cat#12604013
C_{12}FDG	Invitrogen	Cat#D2893
Bafilomycin A_1	Adipogen	Cat# BVT-0252-C100
KOSR	Thermo Fisher Scientific	Cat#10828028
B-27 supplement	Thermo Fisher Scientific	Cat#17504044
N2 supplement	Thermo Fisher Scientific	Cat#17502048
Matrigel	Thermo Fisher Scientific	Cat#3432-005-01
iPS-Brew culture medium	Miltenyi Biotec	Cat#130-104-368
Y-27632 (ROCK inhibitor)	StemCell Technologies	Cat#72308
Dibutyryl-cyclic-AMP	Sigma Aldrich	Cat#sc-201567B
Recombinant Noggin	Preprotech	Cat#6057NG
CHIR99021	LC Laboratories	Cat#C-6556
LDN-193189	Cayman Chemicals	Cat#19396
A83-1	Santa Cruz Biotech	Cat#K1119
Forskolin	LC Laboratories	Cat#F-9929
SB-431542	Cayman Chemicals	Cat#431543
Pyrintegrin	Cayman Chemicals	Cat# 16179

REAGENT or RESOURCE	SOURCE	IDENTIFIER
KC7F2	Cayman Chemicals	Cat# 14123
ZM336372	SelleckChem	Cat# S2720
AZ960	Cayman Chemicals	Cat# 16731
Poly-L-ornithine coating reagent	Sigma Aldrich	Cat#A-004-C
Recombinant human GDNF	R&D Biosystems	Cat#212-GD
Recombinant human BDNF	R&D Biosystems	Cat#248-BDB
Doxycycline	Sigma Aldrich	Cat#089M4004V
BrainPhys culture media	StemCell Technologies	Cat#05790
Triton X-100 reagent	Sigma Aldrich	Cat#X100
DAPI fluorescence reagent for DNA	Sigma Aldrich	Cat#D8417
TURBO DNase for NGS library preparation	Ambion	Cat#AM2238
DNase for cell culture	Roche	Cat#4716728001
TruSeq Stranded mRNA Sample Prep kit	Illumina	Cat#20020594
SYBR Green I for qPCR	Life Technologies	Cat#S7563
SuperScript III First-Strand Synthesis System	Thermo Fisher Scientific	Cat#18080051
Tagment DNA Enzyme and Buffer kit	Illumina	Cat# 20034197
cOmplete EDTA-free Protease Inhibitor Cocktail	Roche	Cat#11836170001
PhosSTOP Phosphatase Inhibitors	Zymo Research	Cat#PHOSS-RO
RIPA Lysis and Extraction Buffer	Thermo Fisher Scientific	Cat#89900
Astrocyte Medium	Sciencell	Cat#1801
Non-Essential Amino Acids (NEAA) supplement	Thermo Fisher Scientific	Cat#M7145
Critical commercial assays		
Click-iT™ Plus TUNEL	Invitrogen	C10618
Cellular Senescence Detection Kit	Biopioneer	CS-001
DNEasy Blood and Tissue kit	Qiagen	Cat# 69504
ProteinSimple 12–230 kDa Separation Module	Bio-Techne	Cat#SM-W004
MethylEPIC BeadChip	Illumina	Cat# 20042130
ProteinSimple Jess 25-Capillary Cartridges	Bio-Techne	Cat#PS-CC01
Deposited data		
iN, Fibroblast, iPSC-iN, and iPSC RNA-Seq and ATAC-Seq raw data	Deposited to ArrayExpress	E-MTAB-10352
iN scRNA-Seq	Deposited to Sequence Read Archive	PRJNA898624
iN Conditioned Media Treated Astrocyte RNA-Seq	Deposited to Sequence Read Archive	PRJNA898624
Experimental models: Cell lines		
Human Astrocytes	ScienCell	Cat#1800
Oligonucleotides		
TruSeq RNA-Seq Single Indexes Set A	Illumina	Cat#20020493
Nextera primers for ATAC-Seq libraries	Buenrostro et al.[75]	N/A
Telomere Standard: TTAGGGTTAGGGTTAGGGTT AGGGTTAGGGTTAGGGTTAGGGTTAGGGTTAG GGTTAGGGTTAGGGTTAGGGTTAGGGTTAGGG	O'Callaghan et al.[38]	N/A

REAGENT or RESOURCE	SOURCE	IDENTIFIER
36B4 Standard: CAGCAAGTGGGAAGGTGTAATC CGTCTCCACAGACAAGGCCAGGACTCGTTTGTA CCCGTTGATGATAGAATGGG	O'Callaghan et al.[38]	N/A
Primer Telo F: CGGTTTGTTTGGGTTTGGGTTTG GGTTTGGGTTTGGGTT R: GGCTTGCCTTACCC TTACCCTTACCCTTACCCTTACCCT	O'Callaghan et al.[38]	N/A
36B4 Primer F: CAGCAAGTGGGAAGGTGTAATCC R: CCCATTCTATCATCAACGGGTACAA	O'Callaghan et al.[38]	N/A
Recombinant DNA		
pLVXUbC-rtTA-Ngn2:2A:Ascl1	Herdy et al.[18]	Addgene #127289
pLVXUbC-rtTA-Ngn2:2A:EGFP	Schafer et al.[76]	Addgene #127288
pCSC-hSyn1::dsRed	Mertens et al.[77]	N/A
pHIV-INK4A-zsGreen	Zeng et al.[78]	Addgene #110728
pLVET-HA-K-RasG12V-IRES-GFP	Zhang et al.[79]	Addgene #107140
pLVX-EF1a-tetOn-IRES-G418 (EtO)	Mertens et al.[77]	Addgene #84776
pLenti CMV p16 *Neo* (w111-1)	pLenti CMV p16 *Neo* (w111-1) was a gift from Eric Campeau	Addgene #22260
Software and algorithms		
STAR	https://github.com/alexdobin/STAR	N/A
HOMER	http://homer.salk.edu/homer/	N/A
DESeq2	https://bioconductor.org/packages/release/bioc/html/DESeq2.html	N/A
RSEM	https://github.com/deweylab/RSEM	N/A
Cellranger	Illumina	N/A
Deeptools	https://deeptools.readthedocs.io/en/develop/	N/A
Bedtools	https://bedtools.readthedocs.io/en/latest/	N/A
Monocle3	https://cole-trapnell-lab.github.io/monocle3/	N/A
FlowJo	https://Flowjo.com/	N/A
GraphPad Prism	https://Graphpad.com/	N/A
RnBeads	https://rnbeads.org/	N/A
ChAMP	http://www.bioconductor.org/packages/devel/bioc/vignettes/ChAMP/inst/doc/ChAMP.html	N/A
Zen Imaging Software	Carl Zeiss	N/A
Fiji	https://ImageJ.net/software/fiji/downloads	N/A
Seurat	https://satijalab.org/seurat/	N/A
Axion Biosystems Neural Module	http://www.axionbiosystems.com/	N/A
RRHO	http://www.bioconductor.org/packages/release/bioc/html/RRHO.html	N/A